Analysis of O_2 Adsorption on Binary−Alloy Clusters of Gold: Energetics and Correlations

Ajay M. Joshi, W. Nicholas Delgass, and Kendall T. Thomson*

School of Chemical Engineering, Purdue University, West Lafayette, Indiana 47907

Received: June 9, 2006; In Final Form: August 29, 2006

We report a B3LYP density-functional theory (DFT) analysis of O_2 adsorption on 27 Au_nM_m (m, $n = 0-3$ and $m + n = 2$ or 3; M = Cu, Ag, Pd, Pt, and Na) clusters. The LANL2DZ pseudopotential and corresponding double-ζ basis set was used for heavy atoms, while a 6-311+G(3df) basis set was used for Na and O. We employed basis-set superposition error (BSSE) corrections in the electronic adsorption energies at 0 K (ΔE_{ads}) and also calculated adsorption thermodynamics at standard conditions (298.15 K and 1 atm), i.e., internal energy of adsorption (ΔU_{ads}) and Gibbs free energy of adsorption (ΔG_{ads}). Natural Bond Orbital (NBO) analysis showed that all the clusters donated electron density to adsorbed O_2 and we successfully predicted intuitive linear correlations between the NBO charge on adsorbed O_2, O−O bond length, and O−O stretching frequency. Although there was no clear trend in the O_2 binding energy (BE = $-\Delta E_{ads}$) on pure and alloy dimers, we found the following interesting trend for trimers: BE (MAu_2) < BE (M_3) ≤ BE (M_2Au). The alloy trimers containing only one Au atom are most reactive toward O_2 while those with two Au atoms are least reactive. These trends are discussed in the context of the ensemble effect and coulomb interactions. We found an approximate linear correlation between the O_2 BE and charge transfer to O_2 for all 27 clusters. The clusters having strongly electropositive Na atoms (e.g., Na_3 and Na_2Au) donated almost one full electron to adsorbed O_2, and the BE is maximum on these clusters. Although O_2 dissociation is likely in such cases, we have restricted this study to trends in the adsorption of molecular O_2 only. We also found an approximate linear correlation between the charge transfer and BE versus energy difference between the bare-cluster HOMO and O_2 LUMOs, which we speculate to be a fundamental descriptor of the reactivity of small clusters toward O_2. Part of the scatter in these correlations is attributed to the differences in the O_2 binding orientations on different clusters (geometric effect). Relatively higher bare-cluster HOMO energy eases the charge transfer to adsorbed O_2 and enhances the reactivity toward O_2. The Frontier Orbital Picture (FOP) is not always useful in predicting the most favorable O_2 binding site on clusters. It successfully predicted the cluster−O_2 ground-state configurations for 10 clusters, but failed for the others. Finally, the energetics of fragmentation suggest that the bare and O_2-covered clusters reported here are stable.

1. Introduction

In the past decade, gold-based catalysts have captured scientific attention due to the dramatic catalytic activity exhibited by nanoscale (<5 nm) Au particles supported on various oxides such as TiO_2, SiO_2, Al_2O_3, and CeO_2, which catalyze important reactions such as low-temperature CO oxidation,[1−6] direct propylene epoxidation with H_2/O_2,[7−18] and the water-gas shift reaction.[19,20] Although bulk gold is least reactive toward important molecules such as H_2,[21] nanogold-based materials can activate a variety of reactant molecules of industrial and academic interest such as O_2, CO, H_2, and alkenes.

Gates and co-workers,[22] based on lack of Au−Au contribution in the EXAFS spectra, reported that the complexes containing cationic single Au atoms supported on NaY zeolite are active in CO oxidation at 298 K. Goodman and co-workers[23] reported that nanometer-sized Au islands on TiO_2 with two layers of gold are most effective for CO oxidation. They attributed the structure-sensitivity of Au-based CO oxidation catalysts to quantum-size effects related to the thickness of Au islands. Some researchers believe that unusually high catalytic activity of highly dispersed Au particles may be in part due to high step densities on small particles and/or strain effects at the cluster−support interface.[24] Electronic interactions with oxide supports can cause charging of Au clusters[25,26] and such charged clusters could also be active in selective oxidation reactions such as CO oxidation and/or propylene epoxidation. In short, there are several proposals to describe the activity of Au-based catalysts and there is no consensus in the literature on which of these effects governs the catalytic activity of supported Au clusters in different reactions or under different conditions. Therefore, there is still a need for experimental and/or theoretical studies aimed at understanding the reactivity of gold nanoparticles—from clusters with few atoms to nanometer-sized particles with hundreds of atoms—and improving the catalytic activity of existing gold-based catalysts.

Although significant advances have already been made through experiments on real catalysts containing oxide-supported Au particles, due to the complexity of materials such as Au/TiO_2 and/or Au/TS-1, it is hard to separate the effects of several important parameters affecting the catalytic activity such as catalyst synthesis variables and pretreatments, known or unknown promoters, Au-particle size-effects, and support-effects. Also, supported Au clusters containing only a few atoms cannot be routinely investigated due to difficulties in experimentally producing, probing, and characterizing such tiny clusters. For direct propylene epoxidation with H_2 and O_2 over Au/TiO_2 catalysts, Haruta and co-workers reported that ∼2−5 nm Au

* Address correspondence to this author. E-mail: thomsonk@ecn.purdue.edu. Phone: (765) 496-6706. Fax: (765) 494-0805.

10.1021/jp063610f CCC: $33.50
Published on Web 10/24/2006

particles are active in the formation of propylene oxide while smaller particles form propane.[7] There is indirect experimental evidence, however, that small few-atom Au clusters likely to be located inside the TS-1 pores (diameter ~5.5 Å) are potentially active in direct propylene epoxidation with H_2 and O_2.[27] Although the geometry and reactivity of supported Au clusters may differ from that of gas-phase clusters, a first step in gaining fundamental insights into Au-based catalysis is to understand the chemistry of the bare (unsupported) Au clusters in the gas phase. This paper focuses on the interaction of O_2 with such small gas-phase clusters since activation of O_2 is a key step in both CO oxidation and propylene epoxidation.

Experimental investigation of the interaction of gas-phase Au_n^- (anion) clusters with O_2 indicated a marked pattern of even−odd reactivity for $n \leq 20$.[28−31] The even-numbered anion clusters adsorb one molecule of O_2 per cluster, while the odd-numbered anions show extremely small or zero reactivity. Mills et al.[32] studied interaction of O_2 with neutral and anionic clusters Au_n ($n = 2-5$) computationally and found that O_2 binds more strongly to clusters having an odd number of electrons than to those with an even number of electrons. Okumara et al.[33] used hybrid density-functional (B3LYP) with LANL2DZ pseudopotential to study binding of O_2 on Au_1 and Au_{13}. On the basis of the Mulliken charge analysis, transfer of some electron density from clusters to adsorbed O_2 was observed.

Since O_2 exhibits high electron affinity, it is likely to accept appreciable electron density from Au clusters. Salisbury et al.[30] have explained that the mechanism of binding involves donation of electron density from anionic Au clusters to the $1\pi_g^*$ molecular orbital of O_2. An even-numbered cluster anion (having an odd number of electrons) can lose one electron relatively easily, forming a closed shell configuration. Adsorbed O_2 with an extra electron obtained from the Au cluster forms a superoxide-like species, which can polarize the Au cluster and hence further stabilize the cluster−O_2 complex. Since odd-numbered cluster anions already have closed shell configurations, electron density transfer to O_2 is not energetically favorable. Consistent with these findings, Wells et al.[34] found that the Frontier Orbital Analysis can help in predicting the strongest binding site and orientation for O_2 on anionic Au_{10}.

Since there is reasonable understanding of Au−O_2 interaction for small Au clusters, as a next step, we recently developed the reaction mechanisms for H_2O_2 formation from H_2 and O_2[35,36] and direct propylene epoxidation that may occur on Au.[37] Hutchings and co-workers have experimentally produced H_2O_2 in liquid phase at low temperature from H_2 and O_2 using Au, Pd, and Au−Pd alloy catalysts supported on various oxides such as Al_2O_3,[38,39] ZnO,[38,39] Fe_2O_3,[40] and TiO_2.[41] They found the highest turn-over frequencies ($TOF_{H_2O_2}$) on Au−Pd alloy catalysts. Goodman and co-workers reported on promotion of Pd catalysts by Au in ethylene acetoxylation to vinyl acetate.[42] Barteau and co-workers have reported increased ethylene oxide (EO) selectivity by alloying Ag catalysts with Cu.[43,44] These studies have generated significant interest in alloy catalysts for important reactions involving O_2. Au−alloy particles in the nanometer-size range can be probed experimentally, as demonstrated by Hutchings and co-workers, who used High-Angle Annular Dark-Field (HAADF) electron microscopy to study the Au/Pd distribution in the alloy particles.[41] Although Greeley and Nørskov[45] have studied O_2 binding on hundreds of binary transition metal alloy surfaces, studies of the reactivity of small Au−alloy clusters toward O_2 are rather scarce.

In this paper, we report a DFT study of binary Au−alloy dimers and trimers containing Ag, Cu, Pd, Pt, and Na as alloy atoms (Au_nM_m): $m, n = 0-3$ and $m + n = 2$ (for dimers) or 3 (for trimers); M = Cu, Ag, Pd, Pt, and Na. For comparison, we also investigated pure dimers and trimers of Au, Ag, Cu, Pd, Pt, and Na. We present the detailed thermochemistry of O_2 adsorption and draw correlations between O_2 binding energy (BE), charge transfer, O_2 stretching frequency, and Highest Occupied Molecular Orbital (HOMO) energies of bare clusters for all 27 clusters. The focus is on O_2 adsorption and activation and does not include O_2 dissociation pathways.

TABLE 1: Comparison of the Calculated and Experimental Properties[a]

molecule	predicted IP[b]	experimental IP
Au_2	9.73	9.16[53]
Au_3	7.27	7.15[53]
Ag_2	7.73	7.60[54]
Ag_3	5.80	6.20[54]
Cu_2	7.94	7.89[55]
Cu_3	5.75	5.78[55]
Pd_2	7.44	
Pd_3	7.53	
Pt_2	9.42	
Pt_3	8.10	
Na_2	5.14	4.91[56]
Na_3	4.07	3.98[56]
molecule	predicted EA[c]	experimental EA
O_2	0.49	0.45[57]

[a] Reference for the experimental data is indicated as a superscript of the value. All the reported values are in electronvolts (eV) [b] IP stands for the ionization potential [c] EA stands for the electron affinity

2. Computational Methods

Our electronic DFT calculations were conducted using the Gaussian 03 suite of programs.[46] We used the 1993 three-parameter hybrid-functional of Becke (B3LYP).[47] In B3LYP, the exchange term is described by the exchange-functional of Becke, the nonlocal correlation is described by the LYP expression,[48] and the local correlation is described by the VWN III functional.[49] We used the Los Alamos LANL2DZ effective core pseudopotential (ECP)[50,51] and the corresponding valence double-ζ basis set for Au, Ag, Cu, Pd, and Pt. The 6-311+G-(3df) basis set was employed for all electrons in O and Na. In what follows, we briefly discuss the rationale behind our choice of DFT functional, pseudopotential, and basis sets.

Due to computer time limitations, calculations including all electrons were out of consideration for Au, Ag, Cu, Pd, and Pt, and the obvious choice was to use an ECP. The LANL2DZ ECP was chosen particularly because of the advantage of enabling faster calculations with relatively little compromise on accuracy. In addition, literature reports on heavy elements have emphasized strong relativistic effects, and the LANL2DZ pseudopotential accounts for these effects.[52] To further support our choice of the DFT functional and the pseudopotential, we provide benchmark calculations in Table 1. Since the clusters donate electron density to adsorbed O_2, we present DFT predictions of ionization potential (IP) of clusters and electron affinity (EA) of O_2. All the predicted values are in good agreement with the corresponding experimental values.[53−57] Since the number of electrons change in the IP calculations, we point out that the errors in the predictions of IPs are likely to represent the maximum possible errors due to approximations in the exchange-correlation functional and should not be treated as errors in the energetics reported in this paper.

Oxygen poses special problems. Metiu and co-workers[58] have shown that compared to CCSD(T) calculations, the B3LYP-

TABLE 2: Calculated Data for Adsorption of O_2 on Pure and Au−Alloy Dimers

cluster	M_2 spin-state	$E_{LUMO-Cluster}$[a]	$E_{HOMO-Cluster}$[a]	M_2-O_2 spin-state	BE[b]	BE_{BSSE}[b]	O−O bond dist[c]	O−O freq[d]	$\Delta E_{ads,\,ZPE}$[b]	ΔU_{ads}[b]	$T\Delta S_{ads}$[b]	ΔG_{ads}[b]
Au_2	singlet	−0.144	−0.264	triplet	2.83	1.52	1.21	1574	−2.38	−1.69	−6.44	4.15
AgAu	singlet	−0.117	−0.232	triplet	1.88	1.11	1.21	1579	−1.51	−0.75	−6.31	4.97
Ag_2	singlet	−0.097	−0.204	triplet	0.81	0.27	1.21	1565	−0.57	0.29	−4.82	4.52
CuAu	singlet	−0.110	−0.235	triplet	10.36	7.41	1.23	1432	−9.82	−9.32	−7.27	−2.65
Cu_2	singlet	−0.085	−0.205	triplet	7.82	4.56	1.25	1392	−7.47	−6.87	−6.00	−1.47
PdAu	doublet	−0.153	−0.232	doublet	6.61	5.54	1.23	1404	−5.98	−5.56	−7.56	1.41
Pd_2	triplet	−0.127	−0.193	triplet	26.33	24.31	1.30	1160	−25.55	−25.49	−8.85	−17.23
PtAu	doublet	−0.163	−0.237	doublet	22.80	20.27	1.27	1266	−21.93	−21.70	−8.45	−13.84
Pt_2	triplet	−0.157	−0.241	triplet	12.86	10.41	1.28	1257	−12.11	−11.87	−8.58	−3.89
NaAu	singlet	−0.073	−0.191	triplet	4.00	3.44	1.22	1442	−3.89	−3.08	−5.31	1.64
Na_2	singlet	−0.055	−0.130	triplet	31.92	30.85	1.33	1223	−31.39	−31.09	−6.81	−24.88

[a] In hartrees. [b] In kcal/mol. [c] In Å. [d] In cm^{-1}.

based calculations over-predicted the O_2 binding energy on Au_2^- and Au_3 by 3.50 and 2.50 kcal/mol, respectively.[58] They attributed these discrepancies to the fact that it is notoriously difficult to model the O_2 molecule with quantum-chemical calculations, especially in this case of partially negatively charged O_2. It is well-known that the prediction of O_2 EA is a challenging task.[59,60] One needs to add diffuse functions in the basis set to predict the oxygen electron affinity accurately. Also, a relatively large basis set can improve the accuracy of the adsorption energies. While Metiu and co-workers[58] used a 6-31+G* basis set with diffuse and polarization functions for oxygen, we chose a 6-311+G(3df) basis set, also with diffuse and polarization functions, for O and Na atoms. Using B3LYP/6-311+G(3df) we get excellent predictions of electron affinity of O_2 with only 0.04 eV error (Table 1). The basis set convergence was also tested by recalculating O_2 binding energies on a few test clusters, using a systematically larger basis set (cc-pVTZ, cc-pVQZ, and cc-pV5Z) for O atoms. We found that our results based on the 6-311+G(3df) basis set are in good agreement with the "converged" binding energies based on the cc-pV5Z basis set (Supporting Information). Therefore, the O_2 binding energy values reported here are practically converged to the complete basis set limit. Moreover, our objective is to extract the trends in the O_2 adsorption energies over the series of Au−alloy clusters and since we are studying neutral clusters and not anionic clusters, the DFT predictions are likely to be relatively better because the electron transfer to O_2 is lower. Finally, we also account for the important entropic effects in O_2 adsorption by performing detailed thermochemical calculations as described below.

For bare clusters we considered different geometries, such as linear, symmetric-triangle, and asymmetric-triangle. For each shape, we investigated three to four possible spin states. The spin-shape combination having the lowest energy was regarded as the ground-state cluster and was considered further for O_2 adsorption studies. In all the O_2 adsorption steps, we considered several different orientations or starting geometries, and carried out full geometry optimization at the aforementioned level of theory. We considered both in-plane as well as out-of-plane attacks, and investigated many combinations of distances, angles, and solid angles. We also considered different possible spin states for clusters with O_2 adsorbed on them. Such a consideration of different spin states is crucial to obtain accurate adsorption energies especially due to the fact that the O_2 molecule has a triplet ground state. Thus, we generated an ensemble of different geometries with different spin states and selected the lowest energy state as the ground state to compute the adsorption energetics. Throughout the paper, we report the binding energies calculated as follows: Binding Energy (BE) $= E(\text{Cluster}) + E(O_2) - E(\text{Cluster-}O_2)$, i.e., $\Delta E_{ads} = -\text{BE}$. Here E is the electronic energy calculated at 0 K in a vacuum. Therefore, a positive binding energy means negative ΔE_{ads}, i.e., favorable exothermic adsorption. Similar notation is used for other thermodynamic quantities such as internal energy (U) and Gibbs free energy (G), i.e., if the change in the Gibbs free energy (ΔG_{ads}) is negative then the adsorption is thermodynamically favorable. We employed the counterpoise (single-point) correction method to calculate the basis set superposition errors (BSSE). The electronic energy of adsorption modified with zero-point energy correction is denoted as $\Delta E_{ads,ZPE}$.

The frequency calculations were performed on all the geometries, and we verified that all the frequencies are positive indicating a minimum energy configuration for both bare and O_2-covered clusters. These frequency calculations also provided us with the thermochemical analysis at a pressure of 1 atm and a temperature of 298.15 K, using the ideal gas approximation. We report the ΔU_{ads}, $T\Delta S_{ads}$, and ΔG_{ads} values calculated at these standard conditions. We note that the heat of adsorption (ΔH_{ads}) can be easily calculated by using the ΔU_{ads} and the ideal gas law or by using the ΔG_{ads} and $T\Delta S_{ads}$, and hence we do not separately report it in the paper. We also point out that we did not scale the calculated frequencies and report them as calculated. The Natural Bond Orbital (NBO)[61] charge analysis of the electron population and the Mulliken spin density analysis on each atomic center were performed with the Gaussian 03 suite.[46] We also note that in Gaussian nomenclature, a spin density of 1.0 represents one unpaired electron (doublet) and so on. Annihilation of spin contaminants was carried out by default in Gaussian 03.[46]

3. Results

Since alloying with Cu improved the selectivity of Ag-based EO catalysts,[44] we investigated the effect of alloying Au clusters with Ag and Cu; all three elements are group IB metals. Similarly, following the proven importance of Au−Pd catalysts,[41] we investigated Au−Pd and Au−Pt alloy clusters. Since the electronic configuration of Au is $[Xe].4f^{14}5d^{10}6s^1$, we wanted to study the effect of alloying Au with Na ($[Ne]3s^1$) which also has one unpaired electron in the outermost "s" shell. Combining strongly electropositive Na with strongly electronegative Au is likely to cause significant charge-polarization of the alloy cluster(s). Therefore, we also investigated Au−Na alloy clusters.

Since we found many different stable configurations of adsorbed O_2 on each cluster, we not only report the ground-state configuration of cluster−O_2 complex but also those configurations which are less than 3.00 kcal/mol higher in energy than the ground-state configuration. This is necessary for two reasons: (1) at standard conditions (298.15 K and 1

TABLE 3: Calculated Data for Adsorption of O_2 on Pure and Au−Alloy Trimers

cluster	M_3 spin-state	$E_{LUMO-Cluster}$[a]	$E_{HOMO-Cluster}$[a]	M_3-O_2 spin-state	BE[b]	BE_{BSSE}[b]	O−O bond dist[c]	O−O freq[d]	$\Delta E_{ads,\,ZPE}$[b]	ΔU_{ads}[b]	$T\Delta S_{ads}$[b]	ΔG_{ads}[b]
Au_3	doublet	−0.193	−0.242	doublet	6.99	5.72	1.28	1203	−6.17	−5.83	−11.06	4.64
$AgAu_2$	doublet	−0.132	−0.186	doublet	12.19	10.88	1.30	1187	−11.27	−11.01	−11.03	−0.58
Ag_2Au	doublet	−0.118	−0.167	doublet	21.14	19.63	1.31	1189	−20.27	−19.95	−10.65	−9.89
Ag_3	doublet	−0.138	−0.185	doublet	20.08	18.45	1.30	1191	−19.25	−18.96	−11.45	−8.11
$CuAu_2$	doublet	−0.137	−0.191	doublet	19.41	16.03	1.29	1210	−18.77	−18.30	−10.07	−8.82
Cu_2Au	doublet	−0.114	−0.168	doublet	42.35	37.07	1.33	1151	−41.18	−41.08	−11.17	−30.51
Cu_3	doublet	−0.098	−0.148	doublet	42.58	37.2	1.33	1157	−41.40	−41.35	−11.53	−30.42
$PdAu_2$	singlet	−0.133	−0.214	triplet	11.17	9.68	1.25	1347	−10.64	−9.93	−8.12	−2.40
Pd_2Au	doublet	−0.132	−0.219	doublet	18.13	16.64	1.28	1215	−16.57	−16.65	−11.74	−5.51
Pd_3	triplet	−0.144	−0.198	triplet	17.61	11.34	1.38	888	−16.65	−16.63	−11.39	−5.83
$PtAu_2$	singlet	−0.141	−0.215	triplet	17.65	16.24	1.26	1281	−17.11	−16.46	−8.58	−8.47
Pt_2Au	doublet	−0.137	−0.210	doublet	29.70	28.2	1.32	1042	−28.17	−28.30	−11.77	−17.13
Pt_3	triplet	−0.151	−0.210	triplet	18.08	16.48	1.33	1004	−16.89	−16.87	−11.29	−6.18
$NaAu_2$	doublet	−0.112	−0.170	doublet	20.05	19.03	1.31	1185	−19.26	−18.88	−9.82	−9.66
Na_2Au	doublet	−0.069	−0.121	doublet	58.83	57.25	1.35	1173	−57.97	−57.73	−10.70	−47.63
Na_3	doublet	−0.068	−0.110	doublet	52.07	50.66	1.35	1172	−51.24	−50.99	−11.20	−40.39

[a] In hartrees. [b] In kcal/mol. [c] In Å. [d] In cm^{-1}.

atm), configurations slightly higher in energy than the ground state can have nontrivial population and (2) to acknowledge the occasional ambiguity in identifying the true ground state out of two or more almost degenerate configurations by using DFT calculations. However, all the extensive details of calculated quantities and related analysis presented below pertain only to the ground-state configurations.

All the BE values discussed below are without any BSSE correction. The BSSE-corrected BE (BE_{BSSE}) values and other details can be found in Tables 2 (dimers) and 3 (trimers). We also note that the HOMO ($E_{HOMO-Cluster}$) and LUMO ($E_{LUMO-Cluster}$) energies reported in Tables 2 and 3 are for bare clusters. All the geometries with atom numbers (1, 2, etc.) and important bond lengths/angles are reported in Figures 1 and 2 (dimers) and in Figures 3−7 (trimers). The NBO charges on all the atoms in different geometries (atom numbers correspond to Figures 1 to 7) are listed in Tables 4 (dimers) and 5 (trimers), and the Mulliken spin density values are reported in the Supporting Information. For reference, we note that the calculated gas-phase O_2 (triplet) bond length is 1.20 Å and the calculated (unscaled) O_2 stretching frequency is 1645.6 cm^{-1}. Finally, since there is a lot of published literature on geometries of small clusters, we only refer to the most relevant studies rather than doing a thorough literature survey.

3.1. O_2 Adsorption on Pure and Binary−Alloy Dimers. *3.1.1. Au_2* (*Figure 1, A*). Our calculated Au−Au bond length (2.57 Å) in ground-state (singlet) Au_2 is in excellent agreement with other DFT studies,[32,62] but differs from the experimental value[63] (2.47 Å). Improved predictions can be obtained by employing computationally very expensive counterpoise-corrected CCSD(T) calculations with the PJHN-4f2g1h1i basis set.[64] The ground state for Au_2-O_2 (bent end-on) is a triplet state and the O_2 BE is only 2.83 kcal/mol, while the PW91-based DFT calculations predict higher values.[32,62] However, it is well-known that the PW91-based DFT calculations overpredict the O_2 BE significantly.[62] Our calculated ΔG_{ads} is 4.15 kcal/mol, indicating thermodynamically unfavorable adsorption. We observed a minor change in the O_2 bond length upon adsorption (1.21 Å) implying lack of activation (negligible electron-transfer to O_2) due to the shell-closing effect responsible for the quite high ionization potential (IP) of even-electron, neutral Au_2.[53] Also, most of the Mulliken spin density in triplet Au_2-O_2 is located on the adsorbed O_2 molecule. This particular finding is also applicable to Ag_2-O_2, $AgAu-O_2$, Cu_2-O_2, and $CuAu-O_2$.

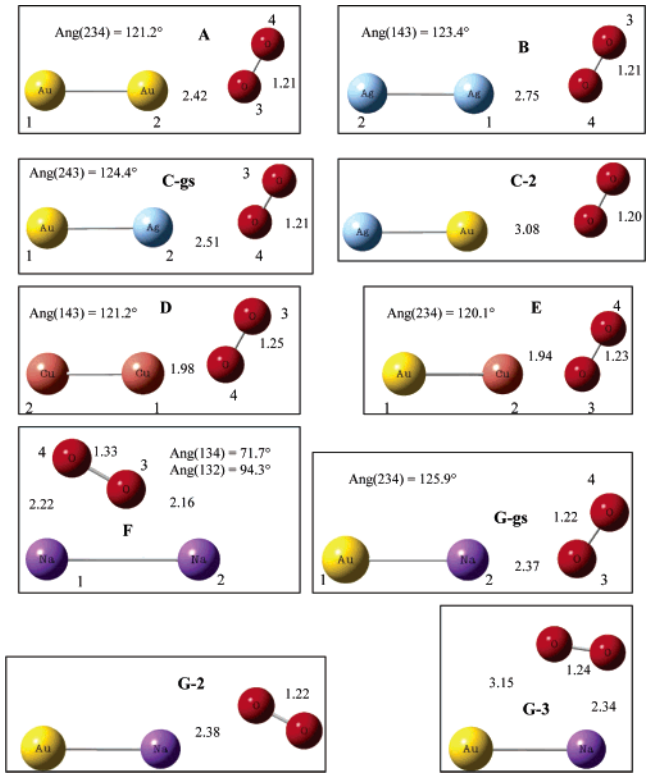

Figure 1. Geometries of O_2 adsorbed on pure and alloy dimers of Ag, Cu, and Na. In all the figures in this paper out-of-plane atoms are indicated by an arrow (↑) on them. All the geometries without any ↑ on atom(s) are planar geometries.

3.1.2. Ag_2 (*Figure 1, B*). Similar to the case for Au_2, our calculations over-predict the Ag−Ag (singlet) bond length. While the calculated value (2.61 Å) agrees well with the DFT literature,[65] the experimentally observed value is somewhat smaller (2.53 Å).[66] O_2 adsorption on Ag_2 is unfavorable with BE = 0.81 kcal/mol and ΔG_{ads} = 4.52 kcal/mol. Again, the O−O bond is only slightly activated (1.21 Å) because of the closed shell configuration of Ag_2.

3.1.3. AgAu (*Figure 1, C*). Significant polarization of the Ag−Au (singlet state) bond occurs due to the much stronger electronegative Au atom withdrawing electron density from the Ag atom (NBO charge on Au is −0.29). The Au−Au bond is significantly shorter (and stronger) than Au−Ag (2.60 Å) and Ag−Ag bonds due to much stronger relativistic effects in Au.[52,67] The O_2 BE on AgAu (1.88 kcal/mol) is between that

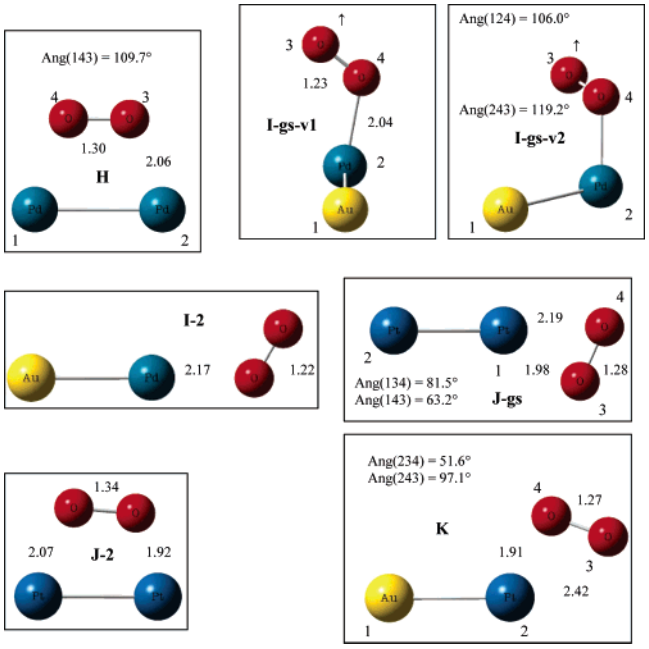

Figure 2. Geometries of O_2 adsorbed on pure and Au−alloy dimers of Pd and Pt. A geometry name X-gs means ground state, X-2/3 means second-/third-most stable state, and X-gs-v1/2 means view no. 1/2 for X-gs.

TABLE 4: NBO Charge Analysis for Adsorption of O_2 on Pure and Au−Alloy Dimers[a]

	NBO charge on each atom				NBO charge
cluster	atom 1	atom 2	atom 3	atom 4	O_2
Au_2-O_2	−0.06	0.081	−0.06	0.039	−0.021
Ag_2-O_2	0.052	−0.017	0.006	−0.042	−0.036
$AgAu-O_2$	−0.313	0.331	0.039	−0.057	−0.018
Cu_2-O_2	0.281	−0.054	−0.042	−0.185	−0.227
$CuAu-O_2$	−0.364	0.529	−0.171	0.006	−0.165
Na_2-O_2	0.606	0.369	−0.591	−0.385	−0.976
$NaAu-O_2$	−0.599	0.769	−0.156	−0.013	−0.169
Pd_2-O_2	0.271	0.271	−0.271	−0.271	−0.542
$PdAu-O_2$	−0.181	0.354	−0.042	−0.132	−0.174
Pt_2-O_2	0.428	−0.143	−0.130	−0.155	−0.285
$PtAu-O_2$	−0.052	0.329	−0.164	−0.113	−0.277

[a] The atom numbers correspond to Figures 1 and 2.

on Au_2 and Ag_2, and negligible electron transfer and minor O−O elongation were also observed. The second-most stable state (C-2: BE = 0.41 kcal/mol) is a triplet state in which O_2 adsorbs on the Au atom while in the ground state (C-gs) it adsorbs on the Ag atom.

3.1.4. Cu_2 (*Figure 1, D*). The ground state of Cu_2 is a singlet with a Cu−Cu bond distance of 2.26 Å, which is in good agreement with the experimental value (2.22 Å)[63] and calculated values.[68,69] The ground state of Cu_2-O_2 is triplet, and we found significant activation of the adsorbed O_2 (O−O bond distance, 1.25 Å) consistent with the relatively higher BE (7.82 kcal/mol) and thermodynamically favorable adsorption (ΔG_{ads} = −1.47 kcal/mol). The calculated NBO charge (−0.23) on adsorbed O_2 indicates easier electron donation by relatively less electronegative Cu_2.

3.1.5. CuAu (*Figure 1, E*). The Cu−Au bond is polarized due to the electronegative Au atom, which acquires significant negative NBO charge (−0.32). Also, the Cu−Au bond length (2.40 Å) in the singlet ground state is between the Cu−Cu and Au−Au bond lengths. Surprisingly, O_2 BE on CuAu (10.36 kcal/mol) is not between that calculated on Cu_2 and Au_2, but is significantly larger, despite significant BSSE correction for $CuAu-O_2$. The ΔG_{ads} is −2.65 kcal/mol and the O−O bond is marginally activated (1.23 Å).

TABLE 5: NBO Charge Analysis for Adsorption of O_2 on Pure and Au−Alloy Trimers[a]

	NBO charge on each atom					NBO charge
cluster	atom 1	atom 2	atom 3	atom 4	atom 5	O_2
Au_3	0.036	0.036	−0.072			
Au_3-O_2	0.300	0.300	−0.108	−0.246	−0.246	−0.492
Ag_3	0.068	0.068	−0.136			
Ag_3-O_2	0.415	−0.138	0.415	−0.346	−0.346	−0.692
Ag_2Au	0.202	0.202	−0.404			
Ag_2Au-O_2	0.560	0.560	−0.414	−0.353	−0.353	−0.706
$AgAu_2$	0.458	−0.229	−0.229			
$AgAu_2-O_2$	0.585	0.285	−0.262	−0.314	−0.293	−0.607
Cu_3	0.148	−0.074	−0.074			
Cu_3-O_2	−0.175	0.474	0.474	−0.387	−0.387	−0.774
Cu_2Au	−0.428	0.214	0.214			
Cu_2Au-O_2	−0.442	0.608	0.608	−0.387	−0.387	−0.774
$CuAu_2$	0.454	−0.227	−0.227			
$CuAu_2-O_2$	0.72	−0.113	−0.113	−0.247	−0.247	−0.494
Na_3	0.009	0.009	−0.018			
Na_3-O_2	−0.336	0.643	0.643	−0.475	−0.475	−0.950
Na_2Au	−0.802	0.401	0.401			
Na_2Au-O_2	−0.830	0.884	0.884	−0.469	−0.469	−0.938
$NaAu_2$	0.830	−0.415	−0.415			
$NaAu_2-O_2$	0.901	0.175	−0.363	−0.328	−0.386	−0.714
Pd_3	0.032	0.032	−0.064			
Pd_3-O_2	0.282	0.263	0.269	−0.416	−0.399	−0.815
Pd_2Au	−0.244	0.122	0.122			
Pd_2Au-O_2	−0.400	0.390	0.390	−0.190	−0.190	−0.380
$PdAu_2$	0.080	−0.040	−0.040			
$PdAu_2-O_2$	0.226	0.031	0.013	−0.183	−0.087	−0.270
Pt_3	−0.044	0.022	0.022			
Pt_3-O_2	0.381	−0.217	0.381	−0.274	−0.274	−0.548
Pt_2Au	0.100	−0.050	−0.050			
Pt_2Au-O_2	−0.216	0.358	0.358	−0.249	−0.249	−0.498
$PtAu_2$	−0.166	0.083	0.083			
$PtAu_2-O_2$	0.125	0.106	0.072	−0.217	−0.086	−0.303

[a] The atom numbers correspond to the Figures 3−7.

3.1.6. Na_2 (*Figure 1, F*). Our calculated Na−Na bond length (3.04 Å) in the singlet ground state of Na_2 is in good agreement with the experimental value (3.08 Å), but pioneering computational studies published many years ago under-predicted the Na−Na bond length (2.91 Å).[70,71] Since Na is strongly electropositive, it is not surprising that the adsorbed O_2 withdraws almost one full electron from Na_2, the BE is 31.92 kcal/mol, and ΔG_{ads} is −24.88 kcal/mol. The O−O bond length in this adsorbed superoxide state (1.33 Å) is close to the calculated value of 1.34 Å for O_2^-. Also, due to strong coulomb attraction, the O atoms stay close to the Na atoms and the adsorbed Na_2-O_2 (triplet) configuration is quite different from that for other dimers. Interestingly, spin density values indicate that one unpaired electron is located on O_2 and the other is located on the Na_2. This means that due to donation of almost one full electron to adsorbed O_2, one electron in Na_2 became unpaired, and the additional electron in O_2 paired with one of the two unpaired electrons (in gas-phase triplet O_2), thus leaving only one unpaired electron on the adsorbed O_2.

3.1.7. NaAu (*Figure 1, G*). Alloying Na with Au results in significant charge-polarization (NBO charge on Au = −0.70) and the Na−Au bond length (2.60 Å) in the singlet ground state is significantly shorter than the Na−Na bond length. Also, we predict a dramatic reduction in the O_2 BE (4.00 kcal/mol) due to alloying with Au. This poisoning of the reactivity of Na toward O_2 by competition of the electronegative Au for the Na 3s electron is accompanied by the negligible elongation of the

O−O bond upon adsorption in the triplet $NaAu-O_2$ complex and the calculated NBO charge on the adsorbed O_2 is only −0.17. Consistent with this reduced charge transfer, the spin density values for $NaAu-O_2$ are more similar to those for $CuAu-O_2$ than for Na_2-O_2. We also report two high-energy configurations G-2 (BE = 3.77 kcal/mol) and G-3 (BE = 2.19 kcal/mol) that are also in the triplet state.

3.1.8. Pd_2 (*Figure 2, H*). In agreement with other DFT studies,[72] we predict a Pd−Pd bond length of 2.53 Å, which, however, is slightly longer than that predicted by using computationally expensive self-consistent-field-configuration-interaction (SCF-CI) calculations (2.46 Å).[73] In agreement with previous studies,[72,74] we found a triplet ground state for Pd_2 where each Pd atom hosts one unpaired electron, i.e., the Mulliken spin density on each Pd atom is 1.00. O_2 adsorbs quite strongly (BE = 26.33 kcal/mol) in a side-on manner to form a triplet Pd_2-O_2 complex. Interestingly, the Mulliken spin density on O and Pd atoms is 0.64 and 0.36, respectively, indicating that even upon O_2 adsorption, Pd_2 prefers to retain significant spin density, and that the spin density on O_2 is probably reduced due to electron transfer from Pd_2.

3.1.9. PdAu (*Figure 2, I*). We found a doublet ground state for this cluster and its bond length (2.56 Å) is only slightly shorter than that calculated for Au_2. The plane-wave-based calculations employing generalized-gradient approximation (GGA) predicted a slightly shorter bond length (2.51 Å).[75] As expected, the Au atom (NBO charge = −0.26) withdraws some electron density from the less electronegative Pd atom. Similar to NaAu, the O_2 BE (6.61 kcal/mol) on PdAu is significantly lower than that calculated for Pd_2. We also note that in the doublet ground state of the $PdAu-O_2$ complex the total Mulliken spin density on O_2 is almost 1.60 and that on PdAu is −0.60. We note that the $PdAu-O_2$ ground state is not planar, but the second-most stable state I-2 (BE = 5.59 kcal/mol) is planar.

3.1.10. Pt_2 (*Figure 2, J*). Similar to Pd_2 we predict a triplet ground state for Pt_2 and our calculated bond length (2.37 Å) is in excellent agreement with previous DFT studies.[72] We, however, predict that Pt_2 is much less reactive (BE = 12.86 kcal/mol) toward O_2 than Pd_2 due to relatively less electron transfer to adsorbed O_2, consistent with the relatively more electronegative nature of Pt. Although the ground state of Pt_2-O_2 is triplet (like Pd_2-O_2) the adsorbed configuration is quite different from that of Pd_2-O_2. This different behavior of Pt_2 is also reflected in the Mulliken spin densities. In the Pt_2-O_2 complex both Pt_2 and O_2 have a total spin density of almost 1.0. While both the O atoms share the spin density almost equally, the Pt atom proximal to the O atoms exhibits a spin density of only 0.26 indicating a concentration of spin density (0.78) on the distal Pt atom. We also found a second most stable (BE = 10.11 kcal/mol) state J-2, with side-on adsorbed O_2.

3.1.11. PtAu (*Figure 2, K*). Consistent with large relativistic contraction in Au and Pt[52] and the resulting high electronegative character, we found very little charge polarization of the PtAu cluster in its doublet ground state. Our calculated bond length (2.54 Å) is in excellent agreement with the multireference singles + doubles configuration interaction (MRSDCI) calculations.[76] In contrast to the case for PdAu, O_2 interacts quite strongly with PtAu (BE = 22.80 kcal/mol) indicating that the PtAu cluster is more reactive than Pt_2 and Au_2. The Mulliken spin density analysis suggested that one unpaired electron in the doublet $PtAu-O_2$ complex is almost entirely situated on the adsorbed O_2. Surprisingly, although the O_2 binding is significantly stronger on PtAu than that on Pt_2, the extent of charge transfer to adsorbed O_2 and O−O elongation are very similar for PtAu and PdAu. Since both the (negatively charged) O atoms are located close to the positively charged Pt atom, we believe that the coulomb attraction contributes significantly to the BE.

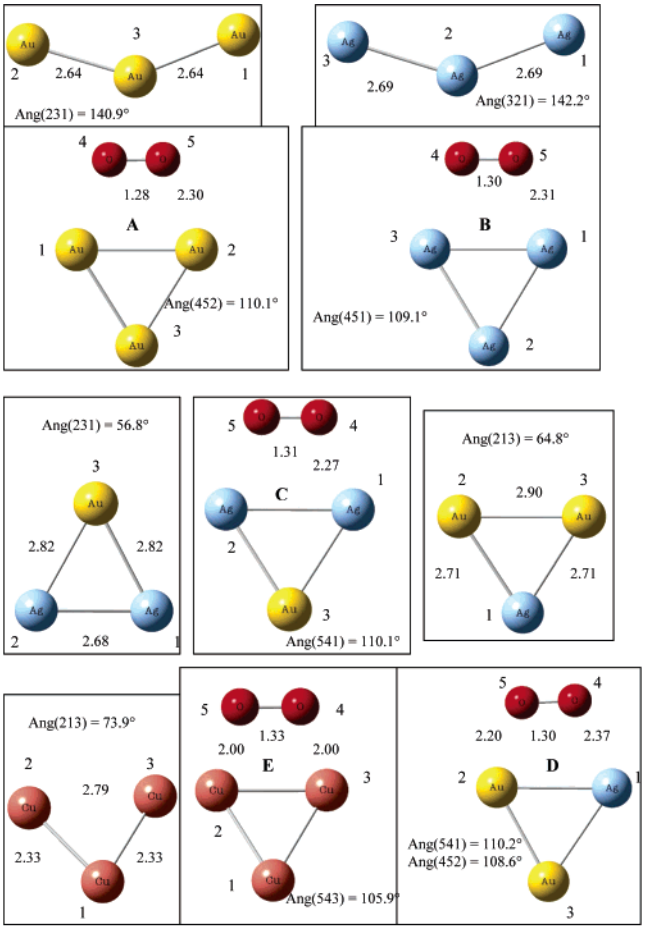

Figure 3. Geometries of O_2 adsorbed on Au_3, Ag_3, Ag_2Au, $AgAu_2$, and Cu_3.

3.2. O_2 Adsorption on Pure and Binary−Alloy Trimers. *3.2.1. Au_3* (*Figure 3, A*). In agreement with both computational[77,78] and experimental studies,[79] we found that the ground state of Au_3 is an obtuse angle (140.9°) triangular geometry (asymmetry due to Jahn−Teller distortions) in the doublet state. Upon O_2 adsorption, in agreement with the DFT literature,[32,62] we found a doublet ground state (BE = 6.99 kcal/mol), which is a planar geometry with side-on bound O_2 hosting one unpaired electron. It should also be noted that the obtuse angle in Au_3 reduces significantly upon O_2 adsorption (63.8°). We found almost −0.50 charge on adsorbed O_2 and also observed corresponding elongation of the O−O bond.

3.2.2. Ag_3 (*Figure 3, B*). There is controversy in the literature on whether the value of the Ag−Ag−Ag obtuse angle in the ground-state configuration is close to 70° or exceeding 140°, as discussed by Matulis et al.[65] We found this angle to be 142° in the doublet ground state. However, irrespective of the starting Ag_3 geometry (70° or 142°), upon O_2 adsorption, we arrived at the same Ag_3-O_2 geometry in the doublet ground state. The O_2 BE (20.08 kcal/mol) is significantly higher than that on Au_3, consistent with the increased electron transfer to O_2 adsorbed on Ag_3. We again found that the unpaired electron is located on adsorbed O_2.

3.2.3. Ag_2Au (*Figure 3, C*). We found a doublet ground state for Ag_2Au with an Ag−Au−Ag angle of 56.8°, which is in

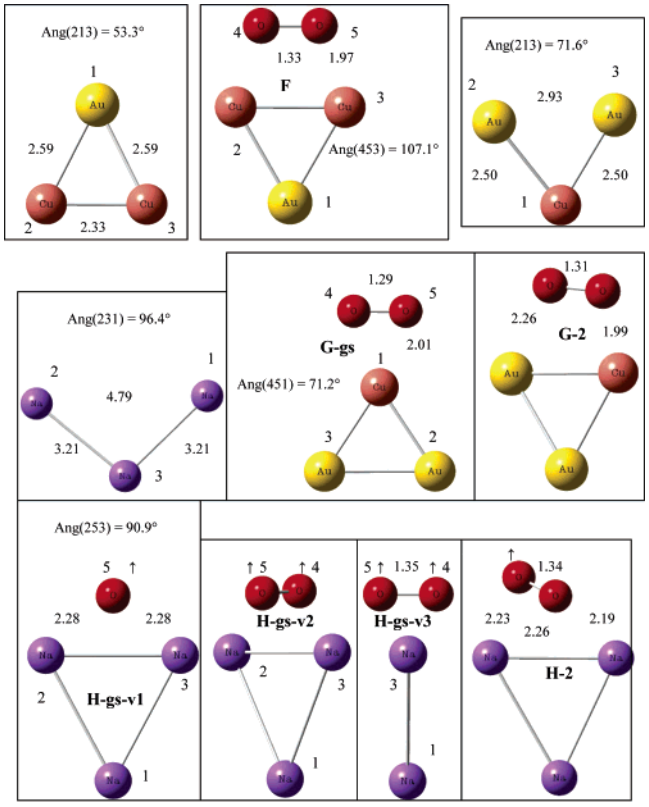

Figure 4. Geometries of O_2 adsorbed on Cu_2Au, $CuAu_2$, and Na_3. A geometry name X-gs means ground state, X-2 means second-most stable state, and X-gs-v1/2/3 means view no. 1/2/3 for X-gs.

reasonable agreement with a previous report.[80] The Au atom exhibits −0.40 NBO charge indicating significant charge polarization. Also, while the Au atom exhibits a Mulliken spin density of almost 0.50, the remaining 0.50 spin density is equally shared by two Ag atoms. Similar to Au_3, the doublet ground state of the Ag_2Au-O_2 complex contains side-on bound O_2. Interestingly, the O_2 BE (21.14 kcal/mol) is slightly increased compared to that of Ag_3.

3.2.4. $AgAu_2$ (*Figure 3, D*). Again, our prediction of Au−Ag−Au angle (64.8°) is consistent with the literature reports.[80] The Ag atom (NBO charge 0.46) loses significant electron density to electronegative Au atoms. The Mulliken spin density on each Au atom is almost 0.50 indicating the delocalization of unpaired electron over two Au atoms. It is interesting to note that the reactivity of $AgAu_2$ is significantly reduced (O_2 BE = 12.19 kcal/mol) compared to that of Ag_2Au and Ag_3, although the extent of charge transfer changes only marginally. The unpaired electron is again located on adsorbed O_2.

3.2.5. Cu_3 (*Figure 3, E*). In agreement with other DFT studies,[68,81] we predict a doublet obtuse angle Cu_3 (73.7°) as the ground state, although there is no consensus in the literature on the exact value of bond lengths and bond angles due to the existence of different, almost degenerate, triangular geometries. As expected, the Cu_3 cluster is very reactive toward O_2 (BE = 42.58 kcal/mol), and forms a doublet Cu_3-O_2 complex with side-on, significantly negatively charged O_2 (NBO charge −0.77), which also hosts one unpaired electron. Again, we arrived at the same Cu_3-O_2 geometry, irrespective of the starting Cu_3 geometry.

3.2.6. Cu_2Au (*Figure 4, F*). Analogous to Ag_2Au, there is a significant charge polarization of the Cu_2Au cluster where the Au atom acquires −0.43 NBO charge and the Cu−Au−Cu bond angle is 53.3° in the doublet ground state. We note that the O_2 adsorption energetics, charge transfer, spin state, and spin density distribution, associated with the Cu_2Au-O_2 complex, are almost same as those for Cu_3.

3.2.7. $CuAu_2$ (*Figure 4, G*). The $CuAu_2$ cluster is an analogue of the $AgAu_2$ cluster; the Au−Cu−Au obtuse angle is about 71.6° and the Cu atom exhibits 0.45 NBO charge in the doublet ground state. Again, due to two Au atoms, the reactivity toward O_2 is substantially poisoned (BE = 19.41 kcal/mol); nevertheless, there is almost half electron-transfer to adsorbed O_2 and the adsorption is thermodynamically favorable ($\Delta G_{ads} = -8.82$ kcal/mol). Interestingly, we found two different $CuAu_2-O_2$ geometries in the doublet state which differ by 2.00 kcal/mol. The ground-state configuration consists of a side-on O_2, bound on the single Cu atom, rather than on one of the two-atom sides. The Mulliken spin density distribution is also unusual with almost 1.40 spin density on the adsorbed O_2 and −0.40 spin density on the metal cluster. The second-most stable state (G-2) contains side-on O_2 bound on the Cu−Au side with the Cu−O distance shorter than the Au−O distance due to stronger coulomb interaction between the Cu atom and the closest O atom.

3.2.8. Na_3 (*Figure 4, H*). We found an obtuse angle (96.4°) doublet ground state for Na_3. Although our predicted longest Na−Na bond length (4.79 Å) matches exactly with the configuration interaction (CI) calculations,[82] there is almost 0.2 Å difference in the (two) shorter Na−Na distances; our DFT method over-predicts this bond length, probably due to electron-correlation effects which are better modeled by the computationally costly CI calculations. Due to the strong electropositive character of Na, we predict almost one full electron transfer to adsorbed O_2 (superoxide). The BE is very high (52.07 kcal/mol), and each negatively charged O atom is equidistant from both positively charged Na atoms, maximizing the coulomb attraction. The O−O bond is perpendicular to the Na−Na bond and both the O atoms are outside the Na_3 plane. However, the spin density distribution is not unusual and the unpaired electron is situated on the adsorbed O_2. We also identified another doublet Na_3-O_2 state (H-2) that is only 1.30 kcal/mol higher in energy than the ground-state Na_3-O_2.

3.2.9. Na_2Au (*Figure 5, I*). We found an obtuse angle (68.6°) ground state (doublet) for Na_2Au where the Au atom exhibits −0.80 NBO charge due to its strong electronegative character. Similar to the trend observed for Ag_2Au/Ag_3, the O_2 adsorption (BE = 58.83 kcal/mol) on Na_2Au is stronger compared to that for Na_3 and the orientation of adsorbed O_2 is similar to that on Na_3-O_2. In the series of 27 clusters reported here, the O_2 adsorption is most favorable ($\Delta G_{ads} = -47.63$ kcal/mol) on Na_2Au.

3.2.10. $NaAu_2$ (*Figure 5, J*). This cluster is almost an equilateral triangle (Au−Na−Au angle = 60.6°) and the Na atom exhibits +0.83 NBO charge. Although the NBO charge on adsorbed O_2 is −0.71, the O_2 BE (20.5 kcal/mol) is reduced significantly, manifesting the poisoning effect due to two Au atoms also observed for $AgAu_2$ and $CuAu_2$. The O_2 molecule is adsorbed on the Na−Au side in the doublet state $NaAu_2-O_2$ complex and surprisingly, the Au−O distance is shorter than the Na−O distance indicating that in this case the effects of overlapping orbitals overrides the coulomb attraction effects in determining the bond lengths.

3.2.11. Pd_3 (*Figure 5, K*). In excellent agreement with previous DFT studies,[74,83] we found that the ground state of Pd_3 is an obtuse angle (65.4°) geometry in a triplet state. In the triplet ground state of the Pd_3-O_2 complex, the O_2 molecule is located outside the Pd_3 plane. Although the NBO charge on

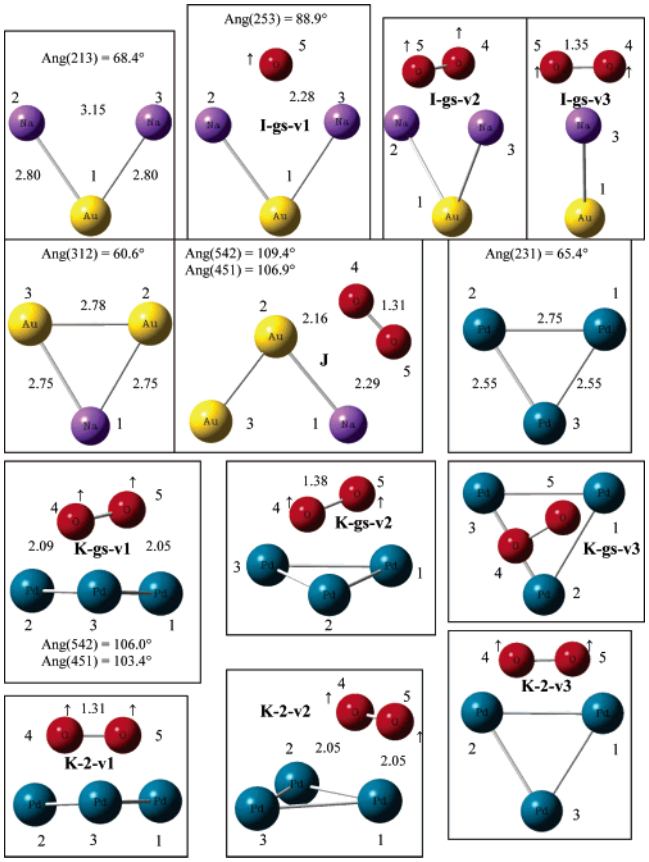

Figure 5. Geometries of O_2 adsorbed on Na_2Au, $NaAu_2$, and Pd_3. A geometry name X-gs means ground state, X-2 means second-most stable state, and X-gs-v1/2/3 means view no. 1/2/3 for X-gs.

adsorbed O_2 is quite negative (−0.82), the BE is relatively low (17.61 kcal/mol) and the BSSE corrections are significantly higher than that found for other clusters in this study. It is interesting to note that in the Pd_3-O_2 ground-state complex there is almost 0.33 spin density on each Pd atom and the second unpaired electron is on adsorbed O_2. We also found another triplet Pd_3-O_2 state, 2.30 kcal/mol higher in energy than the ground state, with O_2 bound in a side-on manner outside the Pd_3 plane.

3.2.12. Pd_2Au (*Figure 6, L*). The Au atom is negatively charged (NBO charge = −0.24) in the doublet ground state of Pd_2Au with a Pd−Au−Pd bond angle of 57.4°. Consistent with the trend reported above, the O_2 BE (18.13 kcal/mol) on Pd_2Au is higher than that on Pd_3, although the extent of electron transfer to adsorbed O_2 is much lower in the Pd_2Au-O_2 doublet ground state with side-on O_2 bound on the Pd−Pd side.

3.2.13. $PdAu_2$ (*Figure 6, M*). In the $PdAu_2$ cluster there is very little charge polarization in the singlet ground state. Also, the cluster is almost an equilateral triangle with a 61.2° Au−Pd−Au angle. Continuing the previously reported trend, the O_2 BE (11.17 kcal/mol) on $PdAu_2$ and the extent of electron transfer to adsorbed O_2 is significantly reduced compared to those of Pd_3 and Pd_2Au. The ground state of the $PdAu_2-O_2$ complex is a triplet state with almost 1.60 spin density on adsorbed O_2, which is bound in a three-dimensional end-on configuration on the Pd atom. We also found another triplet state (M-2) for the $PdAu_2-O_2$ complex that is about 2.50 kcal/mol higher in energy than the ground state and consists of a side-on O_2 bound on the Au−Pd side.

3.2.14. Pt_3 (*Figure 6, N*). We found that Pt_3 triplet is only 0.20 kcal/mol lower in energy than the Pt_3 singlet. Other

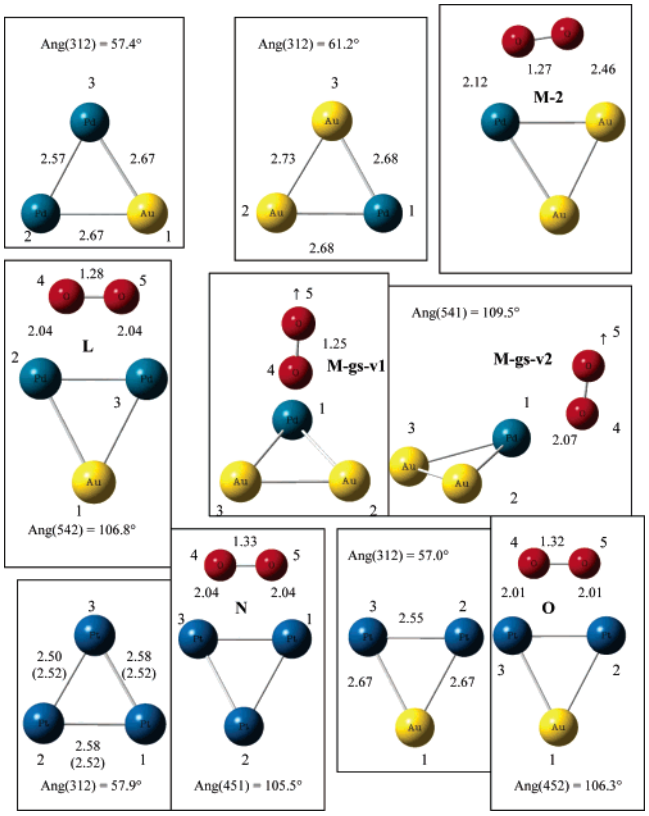

Figure 6. Geometries of O_2 adsorbed on Pd_2Au, $PdAu_2$, Pt_3, and Pt_2Au. A geometry name X-gs means ground state, X-2 means second-most stable state, and X-gs-v1/2/3 means view no. 1/2/3 for X-gs. For Pt_3, bond lengths in parentheses are for the singlet state.

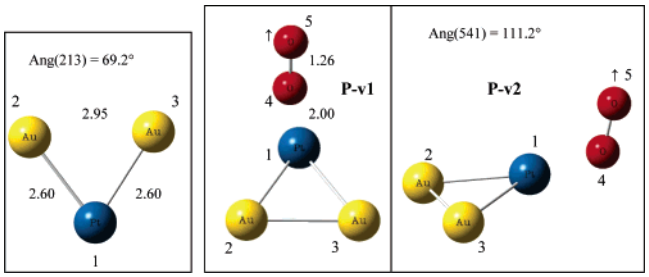

Figure 7. Geometries of O_2 adsorbed on $PtAu_2$. A geometry name X-v1/2 means view no. 1/2 for X.

researchers[84,85] also reported a triplet ground state, but they found an equilateral triangle ground state while we found small deviation from the equilateral triangle geometry in agreement with Grönbeck and Andreoni.[86] The O_2 adsorbs in a side-on manner (BE = 18.08 kcal/mol) and the ground state of Pt_3-O_2 is triplet. Interestingly, the Mulliken spin density on the Pt atom farthest from oxygens is 0.88 and the remaining two Pt atoms each exhibit 0.20 spin density.

3.2.15. Pt_2Au (*Figure 6, O*). We found very little charge polarization in the Pt_2Au cluster in its doublet ground state and the Pt−Au−Pt angle is 57.0°. Again, we found enhanced O_2 adsorption (BE = 29.70 kcal/mol) on this trimer having only one Au atom. The Pt_2Au-O_2 ground state is a doublet state and the majority of the spin density is located on the side-on bound O_2 molecule (similar to the geometry for Pd_2Au-O_2).

3.2.16. $PtAu_2$ (*Figure 7, P*). In the singlet ground state of $PtAu_2$ the Au−Pt−Au angle is 69.2°, i.e., the cluster is an obtuse-angle triangle like $PdAu_2$. Similar to $PdAu_2-O_2$, we found a triplet $PtAu_2-O_2$ ground state with a three-dimensional end-on configuration of O_2 adsorbed on the Pt atom. Again,

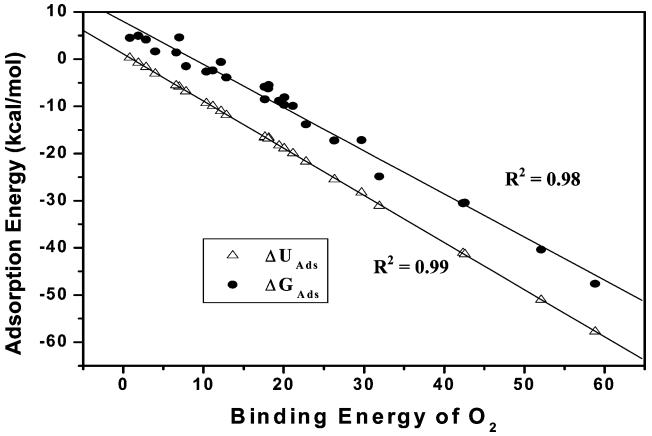

Figure 8. Linear correlation between the O_2 BE and ΔU_{ads} and ΔG_{ads} calculated at standard conditions over the entire range of clusters.

we found that O_2 BE (17.65 kcal/mol) is lower than that on Pt_3 and Pt_2Au and most of the spin density is located on adsorbed O_2.

3.3. Fragmentation of Bare and O_2-Covered Clusters. After identifying the ground-state geometries of bare and O_2-covered clusters, we examined their stability toward fragmentation. We investigated all possible (total 101) combinations in which the clusters might decompose to form smaller clusters or separated constituent atoms. This analysis is relevant to pulsed flow reactor studies in which gas-phase clusters are studied in inert or O_2-containing atmosphere. The energy required for decomposition/fragmentation of bare and O_2-covered clusters (sum of energy of fragments − energy of intact cluster or cluster−O_2 complex) was calculated at the aforementioned level of theory. These data are provided in the Supporting Information. We only note that for all the bare and O_2-covered clusters reported here, the decomposition/fragmentation is not spontaneous, i.e., it is necessary to supply a significant amount of energy to carry out fragmentation. Clearly, all the bare and O_2-covered clusters reported here are more stable than their fragments and hence the stability of these clusters is not a concern.

4. Discussion

4.1. Trends in the Adsorption Energetics. We first point out that over the entire range of clusters, the ΔU_{ads} and ΔG_{ads} correlate linearly (Figure 8) with the O_2 BE and hence all the trends (based on BE) discussed below remain unchanged even when the entropic effects are included in the analysis. Also, since the BSSE corrections are not very different for O_2 adsorption on different clusters, the trends in the BE and BE_{BSSE} are the same. Similarly, trends in the ΔE_{ads} (−BE) and $\Delta E_{ads,ZPE}$ are the same due to relatively small values of zero-point correction to the adsorption energy.

In the case of dimers, we did not find any clear trend in the O_2 BE on M_2 and MAu clusters. While the O_2 BE on AgAu, CuAu, and PtAu is higher than that on Ag_2, Cu_2, and Pt_2, respectively, we found the opposite trend for NaAu/Na_2 and PdAu/Pd_2. Although the electron transfer to adsorbed O_2 is significantly lower for AgAu, CuAu, and PtAu compared to pure dimers, the higher BE on these alloy dimers implies that the extent of electron transfer to O_2 may not alone explain the BE trends. We also note that the O_2 BE trends for Pd_2, PdAu, Pt_2, and PtAu clusters remained unchanged even when systematically larger basis sets (cc-pVTZ, cc-pVQZ, and cc-pV5Z) were employed on O atoms (Supporting Information). Therefore, the lack of overall BE trend for dimers is not due to the basis set limitations.

On the other hand, we found a very interesting trend for trimers: BE (MAu_2) < BE (M_3) ≤ BE (M_2Au). The O_2 BE is slightly enhanced on the alloy clusters with only one Au atom compared to the pure clusters deprived of Au. However, further alloying with Au substantially poisons the reactivity toward O_2 and the O_2 BE is quite low on MAu_2 clusters. The charge transfer to adsorbed O_2 is only marginally different in M_3−O_2/M_2Au−O_2 pairs with the exception of the Pd_3−O_2/Pd_2Au−O_2 pair. However, the charge transfer to adsorbed O_2 is substantially reduced in all MAu_2−O_2 pairs which correlates well with the substantial reduction in the BE. However, the overall correlation between the O_2 BE and the charge transfer to adsorbed O_2 (see below) is not that good. Especially, it is surprising that BE_{M2Au} > BE_{M3}, despite the somewhat higher ionization potential of M_2Au clusters. Interestingly, a qualitative explanation is possible when coulomb interactions based on NBO charges (Table 5) are also analyzed. The negatively charged Au atom in M_2Au units becomes slightly more negatively charged upon O_2 adsorption. The positively charged M_2 atoms in the bare M_2Au clusters become more positively charged upon O_2 adsorption. Clearly, the coulomb interaction between the M_2 unit and adsorbed (negatively charged) O_2 is quite favorable (attractive). Similarly, the coulomb interaction between the M_2 unit and the negatively charged Au is also favorable in both bare and O_2-covered clusters. The geometry of M_2Au−O_2 species is such that the coulomb repulsion between Au and O_2 is minimized as these two species are located on the opposite side of the M_2 unit. Essentially, a positively charged M_2 unit separates negatively charged Au and O_2 species. On the other hand, both Au and M atoms lose electron density to O_2 adsorbed on MAu_2 clusters and overall the coulomb interactions are not as favorable. The coulomb interactions for M_3−O_2 species are approximately between those for M_2Au−O_2 and MAu_2−O_2 species.

The MAu_2 clusters have high ionization potential. Therefore, they donate less electron density to adsorbed O_2. Moreover, coulomb interactions are least favorable for MAu_2−O_2 species. Therefore, O_2 BE is lowest on these clusters. The M_3 and M_2-Au clusters have low ionization potential and adsorbed O_2 withdraws almost the same electron density from these clusters (Table 5). The only exception is the Pd_2Au−O_2 complex. Overall, the main difference in M_3 and M_2Au clusters is the difference in the coulomb interactions upon O_2 adsorption. These interactions are more favorable for M_2Au−O_2 species. Therefore, O_2 BE is only slightly higher on M_2Au clusters than that on M_3 clusters.

We also note that the O_2 molecule prefers to bind on the M_2 subunit of the M_2Au clusters. Therefore, the highest affinity of M_2Au clusters toward O_2 could also be interpreted as an "ensemble" effect. However, for MAu_2 clusters, there is no unique preferred binding site of O_2. On $AgAu_2$ and $NaAu_2$, the O_2 molecule adsorbs on the M-Au side and hence interacts with the Au atom. For the remaining three trimers, however, O_2 prefers to interact with a single M atom and is located quite far from the Au atoms. The BE is lowest on MAu_2 clusters irrespective of whether O_2 is located near Au atoms or not. Therefore, it seems that the ensemble effect alone cannot explain the trend in the BE. In any case, the M_2Au "ensembles" are more reactive toward O_2.

The charge-transfer and coulomb interactions together roughly explain the BE trends on Au−alloy trimers. The ensemble effect is only useful to explain the highest O_2 BE on M_2Au clusters. Nevertheless, it is likely that several interrelated effects such as the ensemble effect, coulomb interactions, and extent of

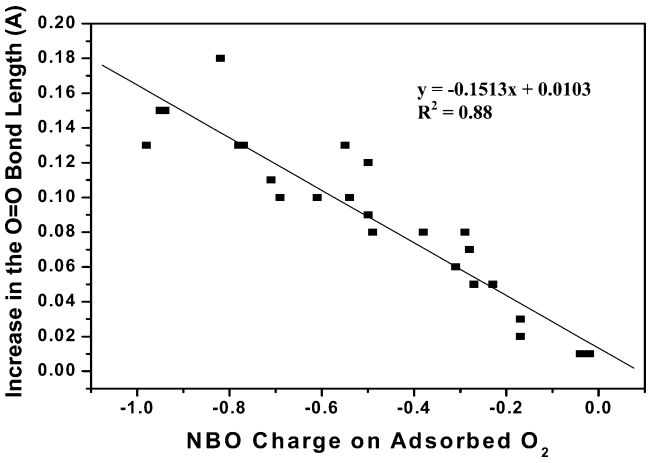

Figure 9. Linear correlation between the increase in the O−O bond length upon adsorption and NBO charge on adsorbed O_2 (data for both dimers and trimers).

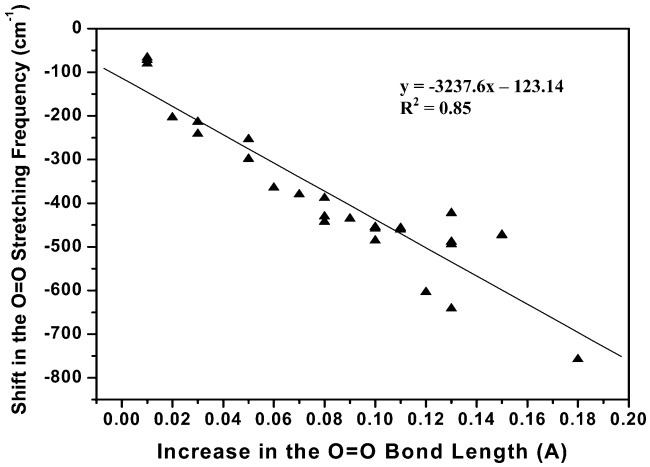

Figure 10. Linear correlation between the increase in the O−O bond length upon adsorption and shift in the stretching frequency (data for both dimers and trimers).

overlap of orbitals are responsible for the observed trends, and quantitative analysis (or deconvolution) of these complex interactions is not easy.

4.2. Investigation of Various Correlations. We first investigated intuitively expected correlations to ensure that our calculations indeed predict physically and chemically meaningful data. We found excellent linear correlation (Figure 9) between the elongation of the O−O bond (upon adsorption) and charge transfer to the adsorbed O_2 molecule. It is interesting that although we have pure/alloy dimers/trimers of six different elements, the correlation is nevertheless good. The red-shift in the O−O stretching frequency upon adsorption also correlates linearly with the elongation of the O−O bond (Figure 10) and hence also with the charge transfer to adsorbed O_2, consistent with the activation of O_2 upon adsorption. This means that by experimentally measuring the stretching frequencies of O_2 on a real catalyst and matching them with the properly scaled computed frequencies, we can easily obtain the molecular-level information such as O−O bond length and charge transfer, based on the correlations reported here. We now discuss our attempts to find good descriptors of reactivity of small clusters toward O_2.

For all the clusters we found that adsorbed O_2 withdraws electron density due to its high electronegativity and undergoes stabilization. This stabilization and the coulomb attraction between the positively charged cluster and the negatively

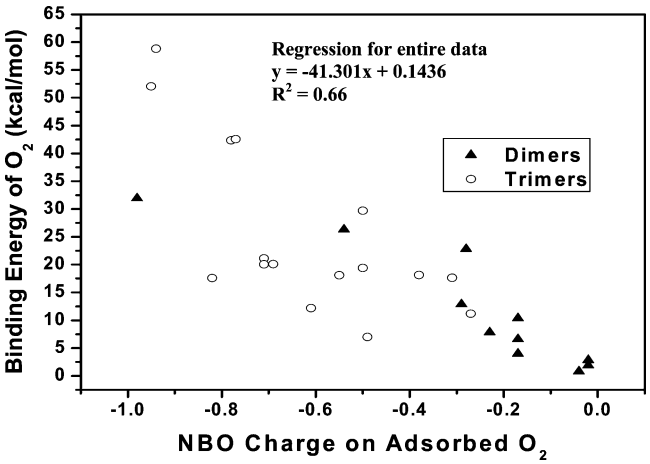

Figure 11. Approximate correlation between the O_2 BE and the charge transfer to the adsorbed O_2 molecule (correaltion for all the data: dimers and trimers).

charged adsorbed O_2 should contribute significantly to the O_2 BE. In fact, we found a decent linear correlation (R^2= 0.66, Figure 11) between the O_2 BE and the NBO charge on adsorbed O_2 by fitting the entire set of data: the more the charge transfer to O_2, the higher the BE. This correlation is better for dimers (individual $R^2 = 0.82$) than trimers (individual $R^2 = 0.52$) and is better in the low BE region than in the high BE region where we found almost one electron transfer to adsorbed O_2. We attribute the scatter in this correlation to the following two factors: (1) variety in the data, i.e., six different elements, pure and alloy clusters, different spin states for bare and O_2-adsorbed clusters, different geometries of adsorbed complexes, and (2) we have not considered the shapes/symmetry of orbitals in bare clusters and O_2 which dictate the extent of overlap of cluster/O_2 orbitals which also contributes to the O_2 BE. As stated earlier, it is difficult to separate the BE contributions of coulomb attraction, charge transfer to O_2, and extent of overlap of relevant orbitals, since all these effects are interrelated in a complex manner and operate simultaneously.

Since the charge transfer to adsorbed O_2 is a rough descriptor of O_2 BE, we examined the relationship of this charge transfer with the energy difference between the bare-cluster HOMO and isolated O_2 LUMOs (Tables 2 and 3). For most of the clusters investigated here, the energy of the bare-cluster HOMO ($E_{\mathrm{HOMO-Cluster}}$) is lower than the energy of O_2 LUMOs ($E_{\mathrm{LUMO-O2}} = -0.126$ hartrees). It is likely that most of the electron density donated to O_2 comes from the HOMO of the bare-cluster, so the extent of this charge transfer is likely to increase with the increase in the HOMO energy. Indeed, we found an approximate linear correlation between the aforementioned energy difference ($E_{\mathrm{HOMO-Cluster}} - E_{\mathrm{LUMO-O_2}}$) and the NBO charge on adsorbed O_2 (Figure 12, $R^2 = 0.69$). Obviously, there is also an approximate linear relationship between the O_2 BE and $E_{\mathrm{HOMO-Cluster}} - E_{\mathrm{LUMO-O_2}}$ (Figure 13).

To examine the sources of scatter in these correlations, we attempted to isolate the geometric effects (Supporting Information). Since we have data for several different binding orientations of O_2 on each cluster, we selected the cluster−O_2 geometries with uniform (similar) binding orientations and examined the aforementioned correlations for dimers and trimers separately. For example, we used the BE and NBO charge data for geometries with O_2 end-on bound on dimers and side-on bound on trimers. We note that some of these geometries are not the ground-state geometries. We made plots of BE versus $E_{\mathrm{HOMO-Cluster}} - E_{\mathrm{LUMO-O_2}}$ and charge transfer versus $E_{\mathrm{HOMO-Cluster}}$

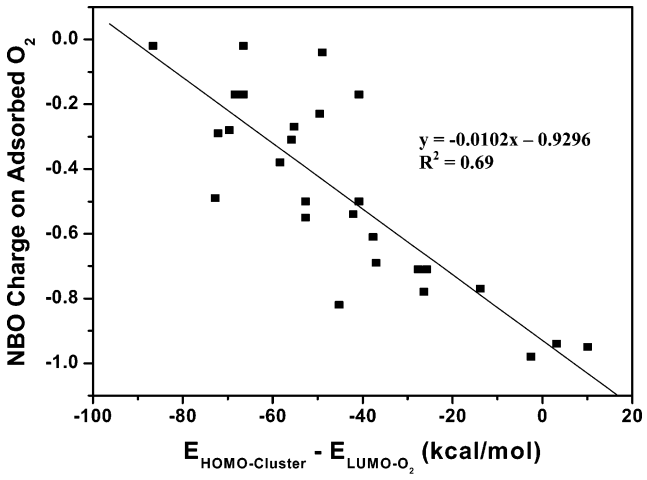

Figure 12. Approximate correlation between the charge transfer to adsorbed O_2 and the $E_{HOMO-Cluster} - E_{LUMO-O_2}$ for bare clusters (data for both dimers and trimers).

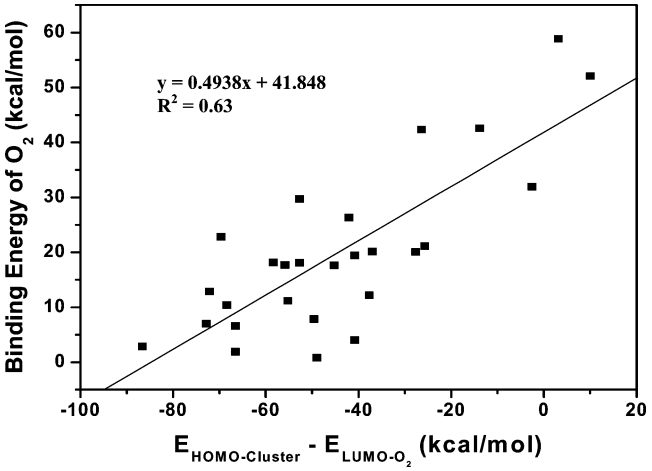

Figure 13. Approximate correlation between the O_2 BE and the $E_{HOMO-Cluster} - E_{LUMO-O_2}$ for bare clusters (data for both dimers and trimers).

$- E_{LUMO-O_2}$ for dimers (end-on O_2) and separately for trimers (side-on O_2). We found that the R^2 values for these correlations (uniform binding orientation of O_2) are somewhat better than the R^2 values corresponding to the data reported here (for ground-state cluster−O_2 geometries). Therefore, part of the scatter in the correlations reported in this paper is due to geometric effects, i.e., due to the differences in the ground-state O_2 binding orientation on different clusters. The factors stated in the previous paragraph may also be responsible for the scatter. In addition, orbitals other than the cluster-HOMO may donate electron density to O_2 and hence the correlation between the NBO charge on O_2 and cluster-HOMO energy is not very precise.

Nevertheless, the bare-cluster HOMO energy level (relative to O_2 LUMO energy) appears to be a fundamental (and easy to calculate) descriptor of the reactivity of different clusters toward O_2. An increase in the bare-cluster HOMO energy level (for most of the clusters: $E_{HOMO-Cluster} < E_{LUMO-O_2}$) reduces the $E_{HOMO-Cluster} - E_{LUMO-O_2}$ gap and leads to easier/enhanced electron transfer to the adsorbed O_2 molecule, which is partly responsible for the increased O_2 BE. We also note that our calculated absolute values (in hartrees) of HOMO and LUMO energies in gas-phase O_2 are −0.320 and −0.126. In fact, for very reactive clusters such as Na_3, Na_2Au, Cu_3, and Cu_2Au, the bare-cluster HOMO energy is only slightly higher or slightly lower than the O_2 LUMO energy, which on the basis of second-order perturbation theory, crudely explains the higher electron transfer to adsorbed O_2 from these clusters (and hence higher BE). Finally, we note that the BE correlates better with the $E_{HOMO-Cluster} - E_{LUMO-O_2}$ than with the cluster IP (correlation not shown here).

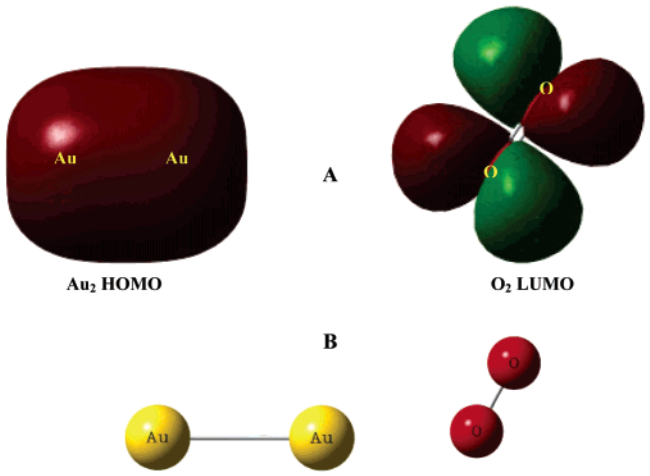

Figure 14. (A) The HOMO of Au_2 and LUMO of O_2 when they are at infinite distance from each other and (B) the geometry of the Au_2−O_2 complex.

By manipulating the nature and number of alloy atoms one can, in principle, increase/decrease the HOMO energy level and hence tune the reactivity toward electron-withdrawing ligands such as O_2. This is true provided the symmetry of the molecular orbitals involved in the interaction is maintained. At this point we also draw the analogy between the bare-cluster HOMO energy and the d-band energy level of the metal surface, which is a very useful descriptor of the reactivity of transition metal surfaces toward O_2.[45] By increasing the d-band energy level for surfaces and bare-cluster HOMO energy for clusters, the reactivity toward O_2 can be enhanced. However, we note that our BE versus $E_{HOMO-Cluster} - E_{LUMO-O_2}$ correlation is only qualitative. This is not surprising because for few-atom clusters the HOMO energy value changes discretely with the total number of atoms and nature/number of alloy atoms, if any. Also, the shapes/symmetry of orbitals in small clusters is quite sensitive to these factors.

4.3. Analysis of Molecular Orbitals. O_2 adsorption on Au clusters involves donation of electron density from the HOMO of Au cluster to the LUMO of O_2. Wells et al.[34] showed that the binding orientation of adsorbed O_2 on Au_{10}^- can be successfully explained using the Frontier Orbital Picture (FOP), i.e., the binding orientation is such that there is maximum favorable overlap between the HOMO of Au_{10}^- and the LUMO of O_2 due to matching of orbital symmetries. Since we observed electron donation from both pure and alloy clusters to the adsorbed O_2 molecule, we now investigate whether binding orientation of O_2 can be explained using the FOP.

4.3.1. Successful Predictions of O_2 Binding Orientation Using the FOP. In Figures 14 and 15 we show HOMOs (isosurface value = 0.02) of Au_2 and Au_3, respectively. By looking at the shape and symmetry of HOMO of Au_2/Au_3 and LUMO of O_2, one can predict the binding orientation of O_2. Indeed we found that the FOP works, and the Au_2−O_2 complex contains an end-on bound O_2 while the Au_3−O_2 complex contains a side-on O_2 bound on the side with the longest Au−Au bond in the bare Au_3 cluster. Also, the shapes of HOMOs of other coinage metal clusters (Ag_2, Ag_3, Cu_2, and Cu_3) are exactly the same (orbitals not shown here) as that of Au_2 and Au_3 and so are the binding

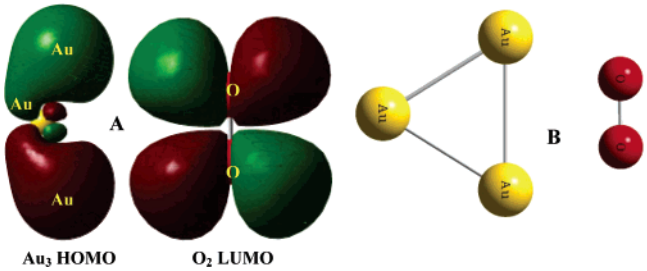

Figure 15. (A) The HOMO of Au_3 and LUMO of O_2 when they are at infinite distance from each other and (B) the geometry of the Au_3-O_2 complex.

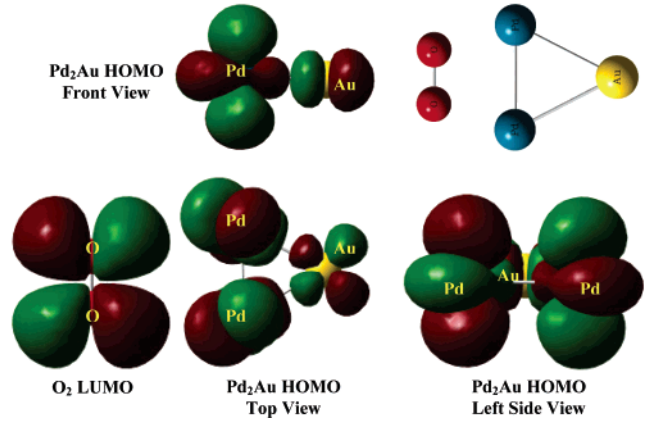

Figure 16. Various views of the HOMO of Pd_2Au and LUMO of O_2 at infinite distance from each other. We also show the Pd_2Au-O_2 complex in its ground-state geometry.

orientations of O_2. Therefore, the FOP also works for Cu and Ag dimers/trimers.

We can also use the FOP to predict the binding orientation of O_2 on Pd_2Au (Figure 16). From the (Top View, Figure 16) Pd_2Au HOMO and O_2 LUMO isosurfaces it is clear that the maximum overlap of orbitals is possible if O_2 binds in a side-on manner on the Pd−Pd side of the cluster and indeed that is the case in the ground-state configuration of Pd_2Au-O_2.

Another interesting case involves O_2 adsorption on $PdAu_2$ where we found two almost degenerate configurations (Figure 6, M-gs and M-2) of the $PdAu_2-O_2$ complex. While the M-gs geometry contains nonplanar end-on O_2 bound on Pd, the M-2 geometry contains planar side-on O_2 bound on the Pd−Au side with the Pd−O distance shorter than the Au−O distance. Looking at the symmetry of the O_2 LUMO and the $PdAu_2$ HOMO (Figure 17) it is clear that the maximum overlap is possible when the $d_{z-square}$ like lobe on Pd interacts with the O_2 LUMO. Therefore, the FOP can explain the nonplanar end-on binding of O_2 in the $PdAu_2-O_2$ ground state. In fact, we can also explain the M-2 geometry. If red (positive wave function) and green (negative wave function) lobes on any one side of the O−O bond overlap with red and green lobes (marked by "x" in blue in the Overall View, Figure 17) of the $PdAu_2$ HOMO then the interaction is favorable. In fact, the green lobe (marked by "x") on Pd is protruding out due to its larger size than the small red lob (marked by "x") on Au. Due to the more favorable local overlap and more attractive local coulomb forces the Pd−O distance is shorter than the Au−O distance.

To avoid redundancy we do not include the isosurfaces of $PtAu_2$ in this paper as the shape/symmetry of $PtAu_2$ HOMO is exactly the same as that of $PdAu_2$ HOMO. In fact, the ground-state configurations of $PtAu_2-O_2$ and $PdAu_2-O_2$ are similar and the FOP can also explain the ground-state geometry of $PtAu_2-O_2$.

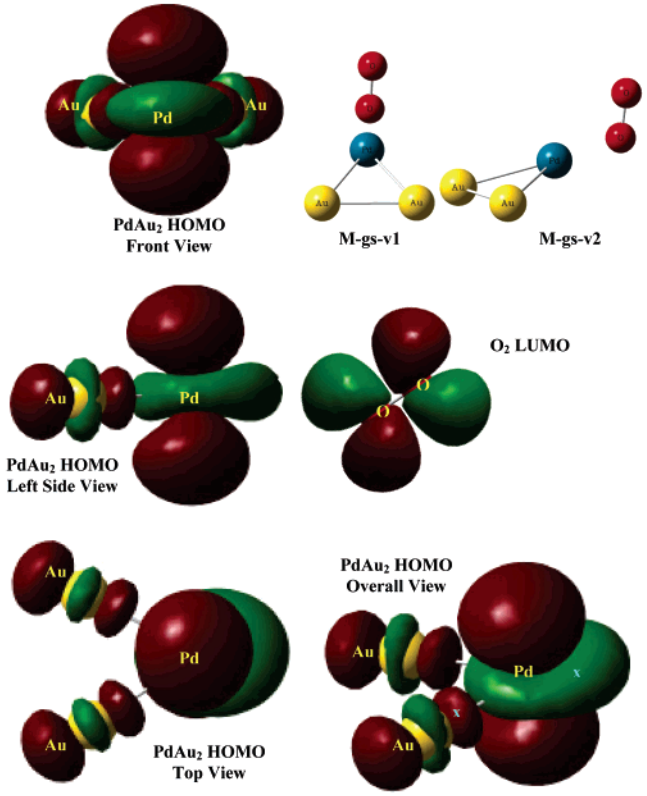

Figure 17. Various views of the HOMO of $PdAu_2$ and LUMO of O_2 at infinite distance from each other. We also show the $PdAu_2-O_2$ complex in its ground-state geometry.

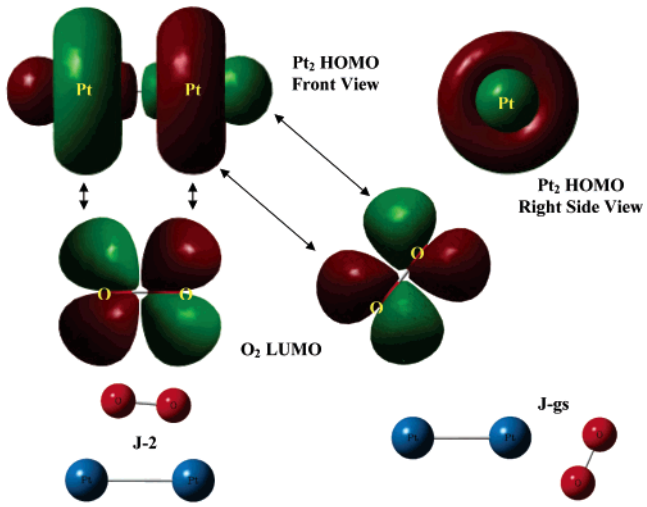

Figure 18. Various views of the HOMO of Pt_2 and LUMO of O_2 at infinite distance from each other. We also show the $Pt-O_2$ complex in its ground state (J-gs) and second-most stable geometry (J-2).

4.3.2. Partially Successful Predictions of O_2 Binding Orientation Using the FOP. The FOP is only partially successful in explaining the ground-state geometry of Pt_2-O_2 (Figure 18). Looking at the shape and symmetry of Pt_2 HOMO and O_2 LUMO one might expect a side-on bound O_2 with equal Pt−O distances in the ground state. However, the almost side-on configuration with surprising unequal Pt−O distances is 2.70 kcal/mol higher in energy than the ground-state Pt_2-O_2. If one considers the small protruding lobe along the Pt−Pt axis together with the ring on the same Pt atom, then it is understandable that these lobes can overlap favorably with the O_2 LUMO and lead to the ground-state configuration of Pt_2-O_2. In addition, based on the favorable interaction between the small protruding

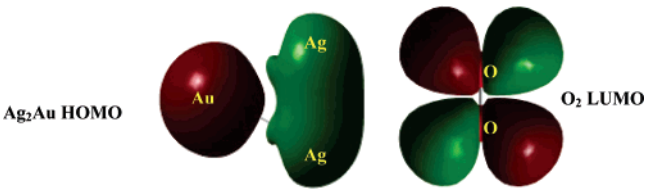

Figure 19. The FOP predicts zero overlap between Ag_2Au−HOMO and O_2−LUMO. Still, the Ag_2Au−O_2 ground state contains side-on O_2 bound on the Ag−Ag side.

lobe along the Pt−Pt axis and the O_2 LUMO, an end-on bound O_2 is also expected. We found that the end-on Pt_2−O_2 complex is 7.60 kcal/mol higher in energy than the ground-state configuration. Therefore, although the FOP is useful in predicting various favorable binding configurations of O_2 adsorbed on Pt_2, an accurate prediction of the actual ground-state configuration cannot be guaranteed.

4.3.3. Failed Predictions of O_2 Binding Orientation Using the FOP. The shape and symmetry of $AgAu_2$ HOMO (not shown here) is exactly the same as that of Au_3 HOMO except that the central atom is Ag. Hence, the FOP predicts a side-on O_2 bound on the Au−Au side in the ground state where maximum favorable overlap is expected. However, such a configuration is 10.00 kcal/mol higher in energy than the ground-state $AgAu_2$−O_2 with side-on O_2 bound on the Ag−Au side where the FOP predicts relatively less overlap of $AgAu_2$ HOMO and O_2 LUMO. Therefore, the FOP fails to predict the ground-state configuration of $AgAu_2$−O_2. The case of $CuAu_2$−O_2 is exactly the same as that of $AgAu_2$−O_2.

Even worse is the case of Ag_2Au. The Ag_2Au HOMO (Figure 19) looks quite different than that of Au_3 and $AgAu_2$. The FOP picture predicts zero net overlap between the O_2 LUMO and the Ag_2Au HOMO (due to both positive and negative wave function of O_2 LUMO overlapping with the positive wave function of Ag_2Au HOMO) if the O_2 molecule adsorbs in a side-on manner on the Ag−Ag side (ground state of Ag_2Au−O_2). In fact, the FOP predicts a side-on O_2 bound on the Ag−Au side, but this configuration is 12.00 kcal/mol higher in energy than the Ag_2Au−O_2 ground state. Similarly, the FOP fails to predict the Cu_2Au−O_2 ground-state configuration.

While we do not discuss the details for the remaining clusters, we note that based purely on the FOP we failed to predict the ground-state configuration of adsorbed O_2 on those clusters. We speculate that the following interrelated complex factors ignored in the Frontier Orbital analysis should be considered to accurately predict the binding orientation of O_2. (1) The cluster HOMO and the O_2 LUMO symmetries may not always match and the orbitals somewhat lower in energy than the cluster HOMO and/or orbitals somewhat higher in energy than the O_2-LUMO may have the right symmetry/shape to overlap favorably and may dictate the O_2-binding orientation. If the cluster−O_2 interaction is strong enough then, in general, not only cluster HOMO and O_2 LUMO, but also orbitals lower/higher in energy may contribute to bonding and the FOP may fail. (2) The coulomb interactions (interrelated to orbitals) may affect the orientation of adsorbed O_2, especially in cases where the extent of charge transfer is substantial (e.g., Na clusters). One should also consider the charge polarization of the bare-alloy clusters due to electronegativity differences in the heteroatoms. (3) It is necessary to carefully examine whether there is any back-donation of electron density from the adsorbed O_2 molecule to the cluster, which may again explain the failure of FOP in some cases. However, we think that it is difficult to separate the effects of various factors stated above and accurate predictions of ground-state cluster−O_2 geometries continue to be a challenge for us.

5. Summary

We have performed DFT calculations augmented with statistical mechanics to obtain detailed energetics of O_2 adsorption on pure and Au−alloy clusters with Ag, Cu, Pd, Pt, and Na atoms as alloy atoms. The energetics of fragmentation suggests that the bare and O_2-covered clusters reported here are stable. Since our objective was to find trends in the energetics of O_2 adsorption over these clusters, we did not consider dissociation of adsorbed O_2. We generated a database comprised of O_2 BE, adsorption thermodynamics, NBO charge analysis, Mulliken spin density analysis, O−O stretching frequencies, O−O bond lengths, and HOMO/LUMO energies of bare clusters, and investigated various correlations using this database. We confirmed that our results are consistent with physically and chemically intuitive correlations such as charge transfer versus O−O bond length/frequency and then we proceeded to identify the descriptors of cluster-reactivity toward O_2.

Over the entire set of pure and Au−alloy dimers we did not find any particular trend in the O_2 BE. However, we found the following interesting trend for trimers: BE (MAu_2) < BE (M_3) ≤ BE (M_2Au). Replacing one atom in the non-Au cluster by Au atom enhanced the reactivity toward O_2. But, further addition of Au poisoned the reactivity toward O_2.

The clusters lose electron density to more electronegative O_2 and the adsorption is stronger and thermodynamically favorable when the extent of electron density donation to adsorbed O_2 is higher. The clusters containing electropositive atoms such as Na obviously donate more electron density to adsorbed O_2 and exhibit the highest reactivity toward it. In fact, the MAu_2 trimers, which are least reactive toward O_2, donate relatively much lower electron density to adsorbed O_2. We found an approximate linear correlation between the O_2 BE and charge transfer to O_2. The charge-transfer and coulomb interactions together roughly explain the BE trends on Au−alloy trimers. The ensemble effect is only useful to explain the highest O_2 BE on M_2Au clusters. However, the extent of favorable overlap between orbitals in the cluster and O_2 also contributes to the BE, which explains why the correlation between BE and charge transfer is not very precise.

Analogous to the d-band energy for the transition metal surfaces, we found a trend in reactivity of small clusters toward O_2 with the bare-cluster HOMO energy ($E_{\mathrm{HOMO-Cluster}} - E_{\mathrm{LUMO-O_2}}$): the higher the HOMO energy and the smaller the $E_{\mathrm{HOMO-Cluster}} - E_{\mathrm{LUMO-O_2}}$ gap, the larger the charge transfer to O_2 and the larger the BE. Although we found only approximate correlations for BE versus $E_{\mathrm{HOMO-Cluster}} - E_{\mathrm{LUMO-O_2}}$ and charge transfer versus $E_{\mathrm{HOMO-Cluster}} - E_{\mathrm{LUMO-O_2}}$, these correlations are better than the BE versus bare-cluster IP correlation (not shown here). This suggests that not only the ability to donate electrons but also the shapes/symmetry of cluster orbitals plays an important role in the cluster−O_2 interaction. We attribute part of the scatter in these correlations to the differences in the O_2 binding orientations on different clusters (geometric effect).

We also carried out an exhaustive study to check whether the Frontier Orbital Picture (FOP) is always useful in predicting the orientation of adsorbed O_2. Since the electron-transfer direction is from clusters to O_2 we looked at the isosurfaces of cluster HOMO and O_2 LUMO. The FOP successfully predicted the ground-state cluster−O_2 configuration for the following

clusters: Au_2, Au_3, Ag_2, Ag_3, Cu_2, Cu_3, Pd_2Au, $PdAu_2$, Pt_2, and $PtAu_2$. In most of these cases the FOP was useful in predicting the second-/third-most stable cluster$-O_2$ configuration as well. However, in some cases such as Ag_2Au, the FOP completely failed in predicting the most favorable site for O_2 adsorption. For the remaining clusters the Frontier Orbital Analysis either only partially succeeded or failed to predict the favorable sites for O_2 adsorption. We speculate that the failure of FOP could be due to involvement of orbitals lower/higher in energy than the HOMO/LUMO, coulomb forces, and, although less likely, due to back-donation of electron density from adsorbed O_2 to cluster. Finally, we note that all these complex effects are interrelated and accurate prediction of the most favorable O_2 binding sites on clusters continues to remain a challenging task.

Acknowledgment. This work was funded by the National Science Foundation through the grant CTS-0238989-CAREER (K.T.T.) and by the United States Department of Energy, Office of Basic Energy Sciences, through the grant DE-FG02-01ER-15107 (W.N.D.). Computational resources were obtained through a grant from the National Computational Science Alliance (AAB proposal ESC030001) and through the supercomputing resources at Purdue University. A.M.J. thanks Yogesh Joshi, Abhijit Phatak, and Dr. Aditya Bhan for their help. The authors thank the peer reviewers for valuable suggestions.

Supporting Information Available: Investigation of the convergence of basis sets with much larger basis sets (cc-pVTZ, cc-pVQZ, and cc-pV5Z); the Mulliken spin density analysis for bare and O_2-covered clusters; details of the fragmentation of bare and O_2-covered clusters; isolation of the geometric effect responsible for the scatter in the correlations reported. This material is available free of charge via the Internet at http://pubs.acs.org.

References and Notes

(1) Guzman, J.; Carrettin, S.; Corma, A. *J. Am. Chem. Soc.* **2005**, *127*, 3286.
(2) Haruta, M.; Yamada, N.; Kobayashi, T.; Iijima, S. *J. Catal.* **1989**, *115*, 301.
(3) Haruta, M.; Tsubota, S.; Kobayashi, T.; Kangeyama, H.; Genet, M. J.; Delmon, B. *J. Catal.* **1993**, *144*, 175.
(4) Haruta, M. *Catal. Today* **1997**, *36*, 153.
(5) Haruta, M.; Daté, M. *Appl. Catal., A* **2001**, *222*, 427.
(6) Guzman, J.; Carrettin, S.; Fierro-Gonzalez, J. C.; Hao, Y.; Gates, B. C.; Corma, A. *Angew. Chem., Int. Ed.* **2005**, *44*, 4778.
(7) Hayashi, T.; Tanaka, K.; Haruta, M. *J. Catal.* **1998**, *178*, 566.
(8) Nijhuis, T. A.; Huizinga, B. J.; Makkee, M.; Moulijn, J. A. *Ind. Eng. Chem. Res.* **1999**, *38*, 884.
(9) Stangland, E. E.; Stavens, K. B.; Andres, R. P.; Delgass, W. N. *J. Catal.* **2000**, *191*, 332.
(10) Mul, G.; Zwijnenburg, A.; van der Linden, B.; Makkee, M.; Moulijn, J. A. *J. Catal.* **2001**, *201*, 128.
(11) Sinha, A. K.; Seelan, S.; Akita, T.; Tsubota, S.; Haruta, M. *Appl. Catal., A* **2003**, *240*, 243.
(12) Chou, J.; McFarland, E. W. *Chem. Commun.* **2004**, 1648.
(13) Cumaranatunge, L.; Delgass, W. N. *J. Catal.* **2005**, *232*, 38.
(14) Nijhuis, T. A.; Visser, T.; Weckhuysen, B. M. *Angew. Chem., Int. Ed.* **2005**, *44*, 1115.
(15) Stangland, E. E.; Taylor, B.; Andres, R. P.; Delgass, W. N. *J. Phys. Chem. B* **2005**, *109*, 2321.
(16) Taylor, B.; Lauterbach, J.; Delgass, W. N. *Appl. Catal., A* **2005**, *291*, 188.
(17) Chowdhury, B.; Bravo-Suárez, J. J.; Daté, M.; Tsubota, S.; Haruta, M. *Angew. Chem., Int. Ed.* **2006**, *45*, 412.
(18) Taylor, B.; Lauterbach, J.; Blau, G. E.; Delgass, W. N. *J. Catal.* **2006**, *242*, 142.
(19) Fu, Q.; Saltsburg, H.; Flytzani-Stephanopoulos, M. *Science* **2003**, *301*, 935.
(20) Sakurai, H.; Akita, T.; Tsubota, S.; Kiuchi, M.; Haruta, M. *Appl. Catal., A* **2005**, *291*, 179.
(21) Hammer, B.; Nørskov, J. K. *Nature* (*London*) **1995**, *376*, 238.
(22) Fierro-Gonzalez, J. C.; Gates, B. C. *J. Phys. Chem. B* **2004**, *108*, 16999.
(23) Valden, M.; Lai, X.; Goodman, D. W. *Science* **1998**, *281*, 1647.
(24) Mavrikakis, M.; Stoltze, P.; Nørskov, J. K. *Catal. Lett.* **2000**, *64*, 101.
(25) Sanchez, A.; Abbet, S.; Heiz, U.; Schneider, W.-D.; Häkkinen, H.; Barnett, R. N.; Landman, U. *J. Phys. Chem. A* **1999**, *103*, 9573.
(26) Joshi, A. M.; Delgass, W. N.; Thomson, K. T. *J. Phys. Chem. B* **2006**, *110*, 16439.
(27) Yap, N.; Andres, R. P.; Delgass, W. N. *J. Catal.* **2004**, *226*, 156.
(28) Cox, D. M.; Brickman, R.; Creegan, K.; Kaldor, A. *Z. Phys. D*: *At., Mol. Clusters* **1991**, *19*, 353.
(29) Lee, T. H.; Ervin, K. M. *J. Phys. Chem.* **1994**, *98*, 10023.
(30) Salisbury, B. E.; Wallace, W. T.; Whetten, R. L. *Chem. Phys.* **2000**, *262*, 131.
(31) Stolcic, D.; Fischer, M.; Ganteför, G.; Kim, Y. D.; Sun, Q.; Jena, P. *J. Am. Chem. Soc.* **2003**, *125*, 2848.
(32) Mills, G.; Gordon, M. S.; Metiu, H. *Chem. Phys. Lett.* **2002**, *359*, 493.
(33) Okumura, M.; Kitagawa, Y.; Haruta, M.; Yamaguchi, K. *Chem. Phys. Lett.* **2001**, *346*, 163.
(34) Wells, D. H.; Delgass, W. N.; Thomson, K. T. *J. Chem. Phys.* **2002**, *117*, 10597.
(35) Wells, D. H.; Delgass, W. N.; Thomson, K. T. *J. Catal.* **2004**, *225*, 69.
(36) Joshi, A. M.; Delgass, W. N.; Thomson, K. T. *J. Phys. Chem. B* **2005**, *109*, 22392.
(37) Joshi, A. M.; Delgass, W. N.; Thomson, K. T. *J. Phys. Chem. B* **2006**, *110*, 2572.
(38) Landon, P.; Collier, P. J.; Papworth, A. J.; Kiely, C. J.; Hutchings, G. J. *Chem. Commun.* **2002**, 2058.
(39) Landon, P.; Collier, P. J.; Carley, A. F.; Chadwick, D.; Papworth, A. J.; Burrows, A.; Kiely, C. J.; Hutchings, G. J. *Phys. Chem. Chem. Phys.* **2003**, *5*, 1917.
(40) Edwards, J. K.; Solsona, B.; Landon, P.; Carley, A. F.; Herzing, A.; Watanabe, M.; Kiely, C. J.; Hutchings, G. J. *J. Mater. Chem.* **2005**, *15*, 4595−4600.
(41) Edwards, J. K.; Solsona, B. E.; Landon, P.; Carley, A. F.; Herzing, A.; Kiely, C. J.; Hutchings, G. J. *J. Catal.* **2005**, *236*, 69.
(42) Chen, M. S.; Kumar, D.; Yi, C.-W.; Goodman, D. W. *Science* **2005**, *310*, 291.
(43) Linic, S.; Jankowiak, J.; Barteau, M. A. *J. Catal.* **2004**, *224*, 489.
(44) Jankowiak, J. T.; Barteau, M. A. *J. Catal.* **2005**, *236*, 366.
(45) Greeley, J.; Nørskov, J. K. *Surf. Sci.* **2005**, *592*, 104.
(46) Frisch, M. J.; Trucks, G. W.; Schlegel, H. B.; Scuseria, G. E.; Robb, M. A.; Cheeseman, J. R.; Montgomery, J. A., Jr.; Vreven, T.; Kudin, K. N.; Burant, J. C.; Millam, J. M.; Iyengar, S. S.; Tomasi, J.; Barone, V.; Mennucci, B.; Cossi, M.; Scalmani, G.; Rega, N.; Petersson, G. A.; Nakatsuji, H.; Hada, M.; Ehara, M.; Toyota, K.; Fukuda, R.; Hasegawa, J.; Ishida, M.; Nakajima, T.; Honda, Y.; Kitao, O.; Nakai, H.; Klene, M.; Li, X.; Knox, J. E.; Hratchian, H. P.; Cross, J. B.; Adamo, C.; Jaramillo, J.; Gomperts, R.; Stratmann, R. E.; Yazyev, O.; Austin, A. J.; Cammi, R.; Pomelli, C.; Ochterski, J. W.; Ayala, P. Y.; Morokuma, K.; Voth, G. A.; Salvador, P.; Dannenberg, J. J.; Zakrzewski, V. G.; Dapprich, S.; Daniels, A. D.; Strain, M. C.; Farkas, O.; Malick, D. K.; Rabuck, A. D.; Raghavachari, K.; Foresman, J. B.; Ortiz, J. V.; Cui, Q.; Baboul, A. G.; Clifford, S.; Cioslowski, J.; Stefanov, B. B.; Liu, G.; Liashenko, A.; Piskorz, P.; Komaromi, I.; Martin, R. L.; Fox, D. J.; Keith, T.; Al-Laham, M. A.; Peng, C. Y.; Nanayakkara, A.; Challacombe, M.; Gill, P. M. W.; Johnson, B.; Chen, W.; Wong, M. W.; Gonzalez, C.; Pople, J. A. *Gaussian 03*, Revision A.1; Gaussian, Inc.: Pittsburgh, PA, 2003.
(47) Becke, A. D. *J. Chem. Phys.* **1993**, *98*, 5648.
(48) Lee, C.; Yang, W.; Parr, R. G. *Phys. Rev. B* **1988**, *37*, 785.
(49) Vosko, S. H.; Wilk, L.; Nusair, M. *Can. J. Phys.* **1980**, *58*, 1200.
(50) Hay, P. J.; Wadt, W. R. *J. Chem. Phys.* **1985**, *82*, 270.
(51) Hay, P. J.; Wadt, W. R. *J. Chem. Phys.* **1985**, *82*, 299.
(52) Bond, G. C.; Thompson, D. T. *Catal. Rev.* **1999**, *41*, 319.
(53) Cheeseman, M. A.; Eyler, J. R. *J. Phys. Chem.* **1992**, *96*, 1082.
(54) Jackschath, C.; Rabin, I.; Schulze, W. *Z. Phys. D*: *At., Mol. Clusters* **1992**, *22*, 517.
(55) Powers, D. E.; Hansen, S. G.; Geusic, M. E.; Michalopoulos, D. L.; Smalley, R. E. *J. Chem. Phys.* **1983**, *78*, 2866.
(56) Peterson, K. I.; Dao, P. D.; Farley, R. W.; Castleman, A. W. *J. Chem. Phys.* **1984**, *80*, 1780.
(57) Rienstra-Kiracofe, J. C.; Tschumper, G. S.; Schaefer, H. F.; Nandi, S.; Ellison, G. B. *Chem. Rev.* **2002**, *102*, 231.
(58) Varganov, S. A.; Olson, R. M.; Gordon, M. S.; Metiu, H. *J. Chem. Phys.* **2003**, *119*, 2531.
(59) Curtiss, L. A.; Redfern, P. C.; Raghavachari, K.; Pople, J. A. *J. Chem. Phys.* **1998**, *109*, 42.
(60) Feller, D.; Davidson, E. R. *J. Chem. Phys.* **1989**, *90*, 1024.

(61) Glendening, E. D.; Reed, A. E.; Carpenter, J. E.; Weinhold., F. *NBO*, Version 3.1*;* Theoretical Chemistry Institute, University of Wisconsin: Madison, WI, 2001.
(62) Ding, X.; Li, Z.; Yang, J.; Hou, J. G.; Zhu, Q. *J. Chem. Phys.* **2004**, *120*, 9594.
(63) Huber, K. P.; Herzberg, G. *Molecular Spectra and Molecular Structure. IV. Constants of Diatomic Molecules*; Van Nostrand: New York, 1979.
(64) Hess, B. A.; Kaldor, U. *J. Chem. Phys.* **2000**, *112*, 1809.
(65) Matulis, V. E.; Ivashkevich, O. A.; Gurin, V. S. *J. Mol. Struct. THEOCHEM* **2003**, *664*−*665*, 291.
(66) Simard, B.; Hackett, P. A.; James, A. M.; Langridgesmith, P. R. R. *Chem. Phys. Lett.* **1991**, *186*, 415.
(67) Pyykkö, P. *Angew. Chem., Int. Ed.* **2004**, *43*, 4412.
(68) Jug, K.; Zimmermann, B.; Calaminici, P.; Köster, A. M. *J. Chem. Phys.* **2002**, *116*, 4497.
(69) Jaque, P.; Toro-Labbe, A. *J. Chem. Phys.* **2002**, *117*, 3208.
(70) Martins, J. L.; Buttet, J.; Car, R. *Phys. Rev. Lett.* **1984**, *53*, 655.
(71) Martins, J. L.; Buttet, J.; Car, R. *Surf. Sci.* **1985**, *156*, 649.
(72) Cui, Q.; Musaev, D. G.; Morokuma, K. *J. Chem. Phys.* **1998**, *108*, 8418.
(73) Estiu, G. L.; Zerner, M. C. *J. Phys. Chem.* **1994**, *98*, 4793.
(74) Nava, P.; Sierka, M.; Ahlrichs, R. *Phys. Chem. Chem. Phys.* **2003**, *5*, 3372.
(75) Sahu, B. R.; Maofa, G.; Kleinman, L. *Phys. Rev. B* **2003**, *67*, 115420.
(76) Dai, D.; Balasubramanian, K. *J. Chem. Phys.* **1994**, *100*, 4401.
(77) Wesendrup, R.; Hunt, T.; Schwerdtfeger, P. *J. Chem. Phys.* **2000**, *112*, 9356.
(78) Bravo-Pérez, G.; Garzón, I. L.; Novaro, O. *J. Mol. Struct. THEOCHEM* **1999**, *493*, 225.
(79) Howard, J. A.; Sutcliffe, R.; Mile, B. *Surf. Sci.* **1985**, *156*, 214.
(80) Bonačić-Koutecký, V.; Burda, J.; Mitrić, R.; Ge, M.; Zampella, G.; Fantucci, P. *J. Chem. Phys.* **2002**, *117*, 3120.
(81) Calaminici, P.; Köster, A. M.; Russo, N.; Salahub, D. R. *J. Chem. Phys.* **1996**, *105*, 9546.
(82) Bonačić-Koutecký, V.; Fantucci, P.; Koutecký, J. *Phys. Rev. B* **1988**, *37*, 4369.
(83) Cui, Q.; Musaev, D. G.; Morokuma, K. *J. Phys. Chem. A* **1998**, *102*, 6373.
(84) Lin, X.; Ramer, N. J.; Rappe, A. M.; Hass, K. C.; Schneider, W. F.; Trout, B. L. *J. Phys. Chem. B* **2001**, *105*, 7739.
(85) Kua, J.; Goddard, W. A. *J. Phys. Chem. B* **1998**, *102*, 9481.
(86) Grönbeck, H.; Andreoni, W. *Chem. Phys.* **2000**, *262*, 1.